Received: 12 February 2021 | Accepted: 1 October 2021

DOI: 10.1111/jmg.12642

ORIGINAL ARTICLE

Journal of METAMORPHIC GEOLOGY WILEY

H_2O in omphacite of quartz and coesite eclogite from Erzgebirge and Fichtelgebirge, Germany

Jürgen Gose | **Esther Schmädicke**

Geozentrum Nordbayern, University Erlangen-Nürnberg, Erlangen, Germany

Correspondence
Esther Schmädicke, Geozentrum Nordbayern, University Erlangen-Nürnberg, Schlossgarten 5a, D-91054 Erlangen, Germany.
Email: esther.schmaedicke@fau.de

Funding information
Deutsche Forschungsgemeinschaft, Grant/Award Number: Schm1039/9-3

Handling Editor: Dr. Bernardo Cesare

Abstract

Major and trace elements in omphacite, including hydrogen, were determined in eclogites from two Variscan basement complexes in Germany: Erzgebirge (EG) and Fichtelgebirge (FG). Erzgebirge eclogite is derived from three units, showing different peak pressure (P) and temperature (T) conditions (Unit 1: 840–920°C/≥30 kbar, Unit 2: 670–730°C/24–26 kbar, Unit 3: 600–650°C/20–22 kbar). The peak conditions of FG eclogite (690–750°C/25–28 kbar) resemble those of EG Unit 2. Coesite eclogite occurs in EG Unit 1, and quartz eclogite in all other units. Omphacite from all samples shows four infrared (IR) absorption bands. Two prominent, sharp bands occur at 3,455 ± 10 cm^{-1} (band II) and 3,522 ± 10 cm^{-1} (band III). Band II is usually more prominent than band III, except for few samples with low jadeite content. A further, broad band is centred between 3,270 and 3,370 cm^{-1} (band I) and a fourth, minor band at 3,611–3,635 cm^{-1} (band IV). Bands II and III are due to hydrogen bound as structural OH^- ions in omphacite. In most cases, this also applies to band IV. However, some spectra with extremely large type IV bands reflect phengite inclusions. The ambiguous band I may be due to different H_2O species (molecular water, structural OH, and water in phengite). Omphacite of quartz eclogite has lower contents of TiO_2, Zr, Hf, and REE, compared with that from coesite eclogite. By contrast, omphacite in quartz eclogite from both EG (H_2O sample averages: 465–852 ppm) and FG (546–1,089 ppm) contains the same amount of structural OH (concentrations given in wt.-ppm H_2O) as omphacite in coesite eclogite (492–1,140 ppm). The obtained difference in the garnet-omphacite H_2O partition coefficient between quartz (0.01–0.03) and coesite eclogite (0.08–0.11) results from different H_2O contents in garnet (coesite eclogite: 50–150 ppm; quartz eclogite: <2–50 ppm; Gose & Schmädicke, 2018). The total content of structural OH in omphacite is unrelated to its major and trace element composition. However, treating the individual IR bands separately, a relation between OH and mineral composition is observed. The OH amount defined by band II is positively correlated to Ti and tetrahedral Al, and that of band III shows a positive correlation with Ca

and a negative one with Na (and jadeite). Both the total OH content of omphacite and the partial contents deduced from individual IR bands are unrelated to PT conditions. This implies that omphacite incorporated its structural H_2O mainly in the quartz stability field, presumably during initial omphacite growth. Conversely, most OH in garnet was derived from the final breakdown of the last remaining calcic amphibole close to or within the coesite stability field. Our data suggest that coesite eclogite is able to transport a significant amount of H_2O (average 550 ppm, maximum 730 ppm), corresponding to that in 3–4 vol.% calcic amphibole, via subduction to depths beyond 100 km. However, the majority of water liberated by dehydration reactions during subduction, including the breakdown of 5–10 vol.% eclogite facies and >10 vol.% pre-eclogitic hydrous minerals, is not preserved in eclogite but liberated to the mantle wedge.

KEYWORDS
eclogite, Erzgebirge, omphacite, structural H_2O, subduction

1 | INTRODUCTION

Significant quantities of hydrogen can be stored in the upper mantle in nominally anhydrous minerals (NAMs) such as olivine, orthopyroxene, clinopyroxene, and garnet (e.g., Bell & Rossman, 1992a, 1992b; Miller et al., 1987) as structural OH^- ions. On the other hand, hydrogen is an incompatible element (e.g., Danyushevski et al., 2000) that is extracted from the mantle by partial melting and, over geologic times, the H content of residual mantle minerals declines. Subduction is the only possibility to counterbalance this continued depletion and to re-fertilize the mantle by adding H_2O, but it remains uncertain if the H and, thus, the H_2O budget of the mantle remains more or less constant, increases, or decreases. In this context, it is important to constrain the amount of H_2O that is added to the mantle via subduction of oceanic crust. To this end, it is critical to evaluate how much H_2O can be stored in the basaltic portion of deeply subducted oceanic slabs.

Most hydrous minerals present in oceanic crustal rocks break down during subduction at relatively shallow depth releasing their water to the mantle wedge, because at low pressure (P) and temperature (T) conditions, little H_2O is storable in NAMs. The H_2O storage capacity of most NAMs present in metabasaltic and peridotitic rocks is usually pressure enhanced (e.g., Grant et al., 2006; Grant et al., 2007; Hirschmann et al., 2005; Kohlstedt et al., 1996; Lu & Keppler, 1997; Rauch & Keppler, 2002; Withers & Hirschmann, 2007), but some studies show that H_2O contents may initially increase with pressure and then decline if pressure exceeds a certain value (Bromiley & Keppler, 2004; Withers et al., 1998). The most important hydrous mineral of metabasaltic rocks—calcic amphibole—is stable to depth of ~100 km, only phlogopite may survive up to 200 km depth (e.g., Frost, 2006; Green et al., 2014; Niida & Green, 1999; Pawley & Holloway, 1993). However, the role of phlogopite for water transport is negligible because MOR (mid-ocean ridge) basalt is too poor in potassium to allow for phlogopite formation. Accordingly, calcic amphibole is the most important H_2O carrier down to 100 km depth, beyond which water transport depends on the amount of H_2O stored in the NAMs present in eclogitized oceanic crust, namely, omphacite and garnet.

Studies on structural OH (hereafter, also designated as structural H_2O; concentrations given in wt.-ppm H_2O) incorporated in omphacite and garnet from both orogenic and xenolithic eclogites (e.g., Huang et al., 2014; Katayama et al., 2006; Koch-Müller et al., 2004; Schmädicke et al., 2015; Schmädicke & Gose, 2017; Skogby et al., 2016) show that omphacite usually hosts considerably more H_2O than garnet. However, the reported H_2O contents in omphacite from natural rocks are highly variable extending over two orders of magnitude (i.e., 30 to 3,000 wt. ppm; Koch-Müller et al., 2007). Such variable contents could be due to differential H_2O loss (Koch-Müller et al., 2007), different mineral composition, different PT peak conditions, and/or different PT paths. The latter govern both the specific PT conditions of dehydration reactions and the sequence of the disappearance of hydrous minerals and simultaneously control the capability of omphacite and garnet to incorporate the liberated water as structural OH (Gose & Schmädicke, 2018).

In the present investigation, omphacite from both orogenic quartz and coesite eclogite is studied to find its capacity to incorporate the water liberated by decomposing

hydrous minerals (such as zoisite and calcic amphibole). To this end, comparison of samples with different PT peak conditions and various eclogite facies mineral assemblages is needed in order to address the following questions: (1) Is there a systematic difference in H_2O concentration between quartz and coesite eclogite? (2) Is the H_2O content in omphacite related to its composition? (3) Are there any characteristics, particularly specific bands, in the infrared (IR) absorption spectra that can be attributed to mineral composition and/or equilibrium PT conditions? (4) Is the partitioning of H_2O between omphacite and garnet governed by PT conditions and/or composition?

The Erzgebirge, Saxony, is an ideal target area to pursue these topics because it hosts three separate eclogite-bearing units (Units 1, 2, and 3; Figure 1), each of which experienced distinct eclogite facies peak PT conditions. These conditions increase from Unit 3 to Unit 1 and encompass a large temperature range of some 300°C and a pressure range of >10 kbar. Two of the units are high-pressure (HP) units with quartz eclogite in which calcic amphibole and zoisite (±phengite) remained stable at peak metamorphic conditions. The third, ultra-high-pressure (UHP) unit contains coesite eclogite, which experienced peak conditions beyond the stability field of calcic amphibole (Schmädicke et al., 1992). In addition to samples from all three Erzgebirge units, quartz eclogite from Fichtelgebirge, Bavaria, is included for comparison, which is very similar to Erzgebirge eclogite from Unit 2 (e.g., Gose & Schmädicke, 2018) and in which calcic amphibole (±zoisite, ±phengite) is part of the metamorphic peak assemblage. Samples from all four units were included to determine the H_2O content in omphacite and its major, minor, and trace element composition. The corresponding data for garnet were recently obtained for the same set of samples (Gose & Schmädicke, 2018; Schmädicke & Gose, 2017).

2 | GEOLOGICAL SETTING

The *Erzgebirge* (EG) is located in the northern part of the Bohemian Massif, the easternmost exposed crystalline complex of the European Variscan belt. The NE–SW-trending Erzgebirge consists of an 80 km × 40 km large, oval-shaped crystalline complex (Figure 1), enveloped by greenschist facies and lower grade meta-sedimentary sequences. The crystalline basement includes a medium-pressure, monotonous gneiss-migmatite unit devoid of eclogite facies relics and three overlying HP units (Units 1, 2, and 3; Schmädicke et al., 1992). The latter are composed of high-grade quartzofeldspathic gneiss and intercalated, conformal lenses of metabasaltic eclogite. Additionally, in Unit 1, garnet peridotite occurs hosting rare layers or lenses of garnet pyroxenite, garnetite (= meta-rodingite; Schmädicke & Evans, 1997; Schmädicke & Gose, 2020), and, very rarely, metabasaltic eclogite, which was unknown until recently (Schmädicke & Gose, 2020). One sample of this

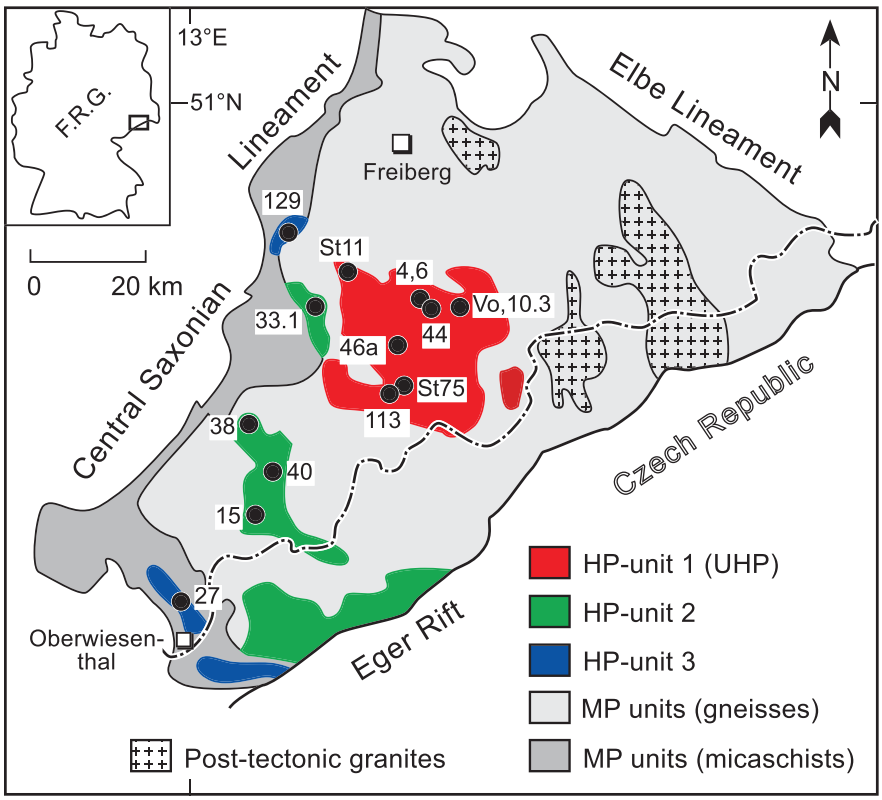

FIGURE 1 Geological map of the crystalline basement of the Erzgebirge (modified after Schmädicke et al., 1995) showing the three high-pressure units and the locations of investigated samples (Table 1). F.R.G., Federal Republic of Germany [Colour figure can be viewed at wileyonlinelibrary.com]

peridotite-hosted eclogite (sample 113) was included while all other samples are from gneiss-hosted eclogite lenses.

The eclogite facies peak conditions show a marked increase from Unit 3 (600–650°C, 20–22 kbar), to Unit 2 (670–730°C, 24–26 kbar), and to Unit 1 (840–920°C, ≥30 kbar; Schmädicke, 1994; Schmädicke et al., 1992). The PT path of Erzgebirge eclogite is hairpin shaped, with peak temperature coinciding with peak pressure. In Units 2 and 3, quartz eclogite occurs, whereas in Unit 1, the UHP conditions led to the formation of coesite-eclogite (Massonne, 2001; Schmädicke, 1991, 1994). Based on the orthopyroxene-bearing assemblages of garnet pyroxenite and peridotite occurring in close vicinity to eclogite (tens of metres apart), the peak pressure for Unit 1 was confined to 33–36 kbar (Schmädicke & Evans, 1997).

Rarely, HP relics also occur in the felsic country rocks. In Unit 1, symplectite of sodian diopside and albite is occasionally present (Schmädicke et al., 1992), and in one locality, microdiamond was found in host-rock gneiss in the vicinity of eclogite lenses (Nasdala & Massonne, 2000; Stöckhert et al., 2001). The petrologic findings imply that eclogite, garnet-bearing ultramafic rocks, and their felsic host rocks are isofacial and experienced a common metamorphic history. The timing of eclogite facies peak metamorphism in the Erzgebirge is constrained by Sm–Nd mineral data (360 ± 7 Ma; Schmädicke et al., 1995) as well as U–Pb zircon data (360.5 ± 5.4 and 359.7 ± 5.3 Ma; Schmädicke et al., 2018).

In the *Fichtelgebirge* (FG), exposed in NE Bavaria, metabasaltic eclogite occurs in the so-called Münchberg Gneiss Complex, which is situated ~100 km to the WSW of the Erzgebirge (Klemd & Schmädicke, 1994). The eclogite-bearing gneiss unit forms the uppermost part of an inverted nappe pile resting on an intermediate medium-pressure gneiss-amphibolite unit, which, in turn, overlies lower grade units at the bottom. The Fichtelgebirge eclogite experienced peak PT conditions of ~ 690–750°C and 25–28 kbar (Klemd & Schmädicke, 1994; O'Brien, 1993), which are very similar to those of eclogite from EG Unit 2. The age of eclogite facies metamorphism (380 Ma), constrained by Sm–Nd and U–Pb dating, is somewhat older compared with that of the Erzgebirge (Gebauer & Grünenfelder, 1979; Stosch & Lugmair, 1990).

3 | PETROGRAPHY

3.1 | General characteristics

Omphacite and garnet are the major minerals in Erzgebirge and Fichtelgebirge eclogite, together making up 90 to 95 vol.% (Table 1). Quartz (or coesite) and rutile invariably occur as minor constituents. The presence of additional, predominantly hydrous, minerals in the peak assemblage depends on PT peak conditions.

Eclogite from both Erzgebirge and Fichtelgebirge is predominantly dark coloured, but a subordinate light-coloured variety is also present. The latter is invariably kyanite bearing and, depending on peak conditions, may also contain a higher proportion of phengite and/or zoisite (compared with dark eclogite). Moreover, omphacite and garnet have very different grain sizes when samples from the different Erzgebirge units and from Fichtelgebirge are compared. The grain size of EG eclogite correlates with the peak temperature and, thus, decreases systematically from Unit 1 with the highest to Unit 3 with the lowest peak T. Accordingly, the grain size of omphacite ranges from ~1–2 mm (Unit 1), via ~0.5 mm (Unit 2), to ~0.1 mm in Unit 3 (Schmädicke, 1994). Fichtelgebirge eclogite with typical omphacite grain sizes of 5–8 mm is invariably much coarser than Erzgebirge eclogite.

Post-eclogitic recrystallization affects eclogite from all units but not all samples. Such secondary overprint is usually restricted to diopside-plagioclase symplectite occurring as rims around omphacite. In many cases, symplectitic breakdown amounts to <5% of the rock volume. In places, secondary amphibole may occur as part of the symplectites, and strongly retrogressed samples may contain amphibole-bearing reaction coronas around garnet but such samples were not included in this investigation.

3.2 | Unit-specific mineral assemblages

In *Erzgebirge* eclogite, the eclogite facies mineral assemblages depend on the unit because, due to the differences in equilibrium conditions, eclogite facies hydrous minerals may or may not be part of the peak metamorphic assemblage. Eclogite from EG *Unit 3*, with the lowest PT peak conditions, contains calcic amphibole, phengite, and zoisite in textural equilibrium with omphacite and garnet. Paragonite only occurs as prograde inclusion. In eclogite from *Unit 2* with higher PT peak conditions, paragonite is absent. Calcic amphibole is part of the peak assemblage and, and most samples, also phengite. In most cases, this also applies to zoisite. However, in some cases, zoisite was not part of the peak assemblage although it was stable during an early (pre-peak) and also during a late (post-peak) eclogite facies stage. In some eclogite specimens, unusually high amounts of calcic amphibole and zoisite (>10 vol.%) are observed. This being the case, the two minerals appear as porphyroblasts (up to 1 cm in size) that overgrew the peak metamorphic

TABLE 1 Modal composition (vol.%) of eclogite samples from Erzgebirge (EG) and Fichtelgebirge (FG) and PT conditions for eclogite facies peak metamorphism

Sample	Locality	Unit	Grt	Omp	Qz	Coe	Rt	Hbl bleb-textured	Hbl	Zo	Phe	Ky	Sym	Comment	T [°C]	P [kbar]
EG																
4	Großwaltersdorf East	EG 1	30	60	6	<1	1	1	–	–	–	–	<1	opq 2		
6	Großwaltersdorf East forest	EG 1	30	54	5	+	2	5	–	?	–	–	2	opq 2		
10.3	Voigtsdorf	EG 1	45	50	2	+	<1	1	–	–	–	–	1	opq +	924	≥30
Vo	Voigtsdorf	EG 1	30	62	5	+	1–2	1	–	–	–	–	–	opq < 1		
St11	Eppendorf	EG 1	30	65	2	<1	1	–	–	–	1–2#	–	–	opq +	892	≥30
St11–2	Eppendorf	EG 1	30	65	5	<1	<1	–	–	–	<1#	–	+	opq +		
St75	Blumenau	EG 1	40	55	3–4	+	<1	2	–	–	+ $	<1	–	phl < 1	870	≥30
113	Zöblitz	EG 1	40	50	3	+	2	4	–	?	–	–	+	opq +	943	≥30
44	Mittelsaida	EG1	30	30	10	+	1	–	+*	–	–	–	30	opq < 1		≥30
46a	Forchheim	EG 1	30	1	10	<1	1–2	–	5*	–	–	–	50	bt 2	837	≥30
15	Mildenau	EG 2	40	45	1	–	1	–	1	10	–	1	–		665	24–26
33.1a	Grünhainichen	EG 2	25	63	2	–	<1	+?	1	3–5	2	–	<1	opq +	667	24–26
38	Wolkenstein	EG 2	30	65	1	–	1	–	1	–	1	–	+	opq +	730	24–26
40	Großrückerswalde	EG2	30	45	2	–	1	–	20**	1	2	–	–	opq +	768	24–26
27	Crottendorf	EG 3	30	45	2	–	3	–	10	+	+	+	–	opq < 1	661	20–22
129	Metzdorf	EG 3	30	45	3	–	<1	–	20	–	–	–	–	opq < 1	602	20–22
FG																
Fa	Fattigau	FG	40	48	3	–	2	–	7	–	–	–	+			
Mt	Martinsreuth	FG	30	57	4	–	2	–	2	2	2	<1	+	opq < 1	720	25–28
Ok	Oberkotzau	FG	30	60	1	–	<1	–	–	5	<1	2	–	opq < 1	690	25–28
Ws	Weißenstein	FG	20	60	5	–	<1	–	3	4	–	7	–	opq < 1	750	25.28

Note: PT conditions for EG eclogite are from Schmädicke (1994), Schmädicke & Müller (2000; sample St75), Schmädicke & Evans (1997; sample 113), and new calculations. Co-facial garnet pyroxenite in Unit 1 points to a peak of 34–35 kbar (Schmädicke & Evans, 1997). P for FG eclogite from O'Brien (1993); T for FG eclogite calculated from data in O'Brien (1993) using the same thermometer as for EG samples. 'Bleb-textured' hornblende with inclusions of vermicular quartz formed during decompression in coesite eclogite at >25 kbar. Symbols: + trace (i.e., <0.1%); * recrystallized from symplectite; ** post-peak porphyroblasts; # prograde inclusion in grt and omp; $ prograde relict replaced by phl.

Abbreviations: bt, biotite; coe, coesite; grt, garnet; hbl, hornblende; ky, kyanite; omp, omphacite; opq, opaque mineral; phe, phengite; phl, phlogopite; qz, quartz; rt, rutile; sym, symplectite; zo, zoisite.

minerals, which points to eclogite facies recrystallization postdating the peak metamorphic stage.

In the UHP eclogite of *Unit 1*, hydrous minerals are not part of the peak assemblage—a fact ascribed to the high peak conditions (e.g., Schmädicke et al., 1992). However, in an exceptional Mg- and Al-rich eclogite (sample St75), phlogopite was formed at peak conditions at the expense of prograde phengite (Schmädicke & Müller, 2000). All other examples of UHP eclogite, known so far, are characterized by a 'dry' peak assemblage, which includes omphacite, garnet, coesite/quartz, rutile, and rare K-feldspar. Calcic amphibole is a typical eclogite facies constituent in samples of Unit 1; however, it formed during post-peak re-equilibration at P = 25–30 kbar, clearly prior to post-eclogitic breakdown of omphacite. This post-peak amphibole occurs in interstitial positions and shows inclusions of vermicular quartz, indicative of formation at the expense of omphacite (Gose & Schmädicke, 2018; Schmädicke et al., 1992; Schmädicke & Evans, 1997). Such textural characteristics are absent in eclogite from Units 2 and 3, in which calcic amphibole remained stable at peak metamorphic conditions. The single sample of peridotite-hosted eclogite (113) is indistinguishable from gneiss-hosted eclogite.

Fichtelgebirge eclogite not only experienced the same PT conditions as eclogite from EG Unit 2 but it is also characterized by the same mineral assemblages (Table 1). Thus, the hydrous minerals calcic amphibole, zoisite, and phengite were stable at peak metamorphism. Paragonite is preserved only as prograde inclusions and reacted to form kyanite at eclogite facies peak conditions.

4 | ANALYTICAL DETAILS

The H_2O content of omphacite present as (i) hydroxyl in the pyroxene structure (referred to as 'structural H_2O') and (ii) as molecular water in fluid inclusions was determined by IR spectroscopy using unpolarized radiation, and contents of both species are given as wt.-ppm H_2O. The same mineral grains were analysed for major, minor, and trace element composition by electron microprobe and laser-ablation ICP-MS analysis. The selection of samples is based on thin section observations. Thin section microscopy was also needed to identify the mineral assemblages and, especially, to find out if hydrous minerals coexisted with omphacite and garnet at metamorphic peak conditions. From the selected samples (Table 1), doubly polished, self-supporting slices (thick sections) were prepared, the thickness of which varies between 0.15 and 0.25 mm, depending on grain size and crystal quality. The thick sections were used for all analytical tasks that were performed in the order (1) IR spectroscopy, (2) electron microprobe analysis, and (3) ICP-MS analysis.

For major element analysis, the JEOL 8200 electron microprobe equipped with five wavelength-dispersive spectrometers was used. Operating conditions of 15 kV and 15 nA and a counting time of 20 to 40 s were applied, and silicate and oxide standards were used for calibration. Three to four omphacite grains were analysed per sample. For each, 5–10 spot analyses were collected from different sites (i.e., core and rim) to unravel possible compositional differences. The analytical error of the results is ≤1% (relative). For elements with concentrations < 2 wt%, the uncertainty is 1–10%. Average analyses for each sample are given in Table 2 and the standard deviations in Table S1.

Trace element analysis was performed with a LA-Q-ICP-MS unit, using an UP193FX laser (New Wave Research) connected to an Agilent 7500i quadrupole inductively coupled plasma mass spectrometer, tuned for maximum sensitivity by ThO/Th < 0.5%. Background and mineral ablation times were 20 and 25 s, respectively, and the spot diameter between 30 and 50 μm. The NIST SRM 612 reference material and the SiO_2 content from microprobe analysis served as external and internal standard, respectively. The BCR-2G (USGS) reference material was used as secondary standard to test reproducibility (mostly <5%) and accuracy (mostly <8%). Data processing was carried out using the GLITTER software (van Achterbergh et al., 2000). For each sample, 4–10 analyses were collected; samples averages are given in Table 3 and standard deviations in Table S2.

The H_2O content of omphacite was determined by Fourier-transform IR spectroscopy utilizing a Bruker Vertex 70 spectrometer at the University of Innsbruck, which is equipped with a Hyperion 3000 microscope, an MCT detector, and a KBr beam splitter. The spectra were obtained by averaging over 32 scans in the wavenumber range 550–7,500 cm^{-1} with an instrumental resolution of 2 cm^{-1}. The samples were analysed with unpolarized IR radiation (transmittance mode) using a square aperture of 30×30 to $100 \times 100\ \mu m^2$ (in most cases $\sim 50 \times 50\ \mu m^2$) to restrict the lateral size of the probed sample volume in order to probe only clear, transparent crystal volumes free of any visible inclusions, cracks, or alteration products. In each sample, 12 to 27 grains were analysed, and for a representative number of grains, spectra were collected from different grain areas (i.e., core and rim). The H_2O content was determined according to a modified Beer–Lambert law, with $A_{total} = 3 \times A_{average}$, following the method outlined by Kovács et al. (2008) and Sambridge et al. (2008). In the case of anisotropic crystals, the determination of absorbances using unpolarized instead of polarized IR radiation produces, due to

TABLE 2 Major element composition of omphacite (sample averages) determined by microprobe analysis

Sample	**4**	**6**	**10.3**	**Vo**	**St11**	**St75**	**113**	**44**	**46a**
Unit	**EG 1**	**EG 1**	**EG 1**	**EG 1**	**EG 1**	**EG 1**	**EG 1**	**EG 1**	**EG 1**
N	**26**	**20**	**25**	**15**	**13**	**28**	**31**	**26**	**35**
SiO_2	55.96	54.97	55.55	55.38	55.59	55.52	55.21	55.46	54.82
TiO_2	0.22	0.21	0.18	0.19	0.15	0.09	0.18	0.21	0.33
Al_2O_3	11.62	13.46	11.07	10.40	11.94	8.71	10.44	12.08	11.68
Cr_2O_3	0.02	0.04	0.04	0.03	0.06	0.07	0.04	0.04	0.02
FeO	4.67	3.00	3.42	5.01	2.99	2.01	4.73	4.04	4.81
MnO	0.03	0.03	0.03	0.03	0.03	0.01	0.03	0.03	0.03
MgO	7.97	8.01	9.61	8.68	8.74	11.98	9.01	8.10	8.43
NiO	0.01s	0.01	0.03	0.02	0.01	0.04	0.02	0.01	0.02
ZnO	0.03	0.03	0.03	0.03	0.04	0.02	0.03	0.05	0.03
CaO	13.08	13.19	15.26	14.33	14.59	17.80	14.80	12.47	14.22
Na_2O	6.95	6.68	5.55	6.23	6.09	4.19	5.85	6.92	6.08
K_2O	0.00	0.00	0.00	0.01	0.01	0.01	0.00	0.00	0.00
Total	100.57	99.63	100.77	100.32	100.24	100.45	100.34	99.41	100.47
Si	1.982	1.949	1.961	1.977	1.965	1.966	1.970	1.978	1.951
Ti	0.006	0.006	0.005	0.005	0.004	0.002	0.005	0.006	0.009
Al	0.485	0.563	0.461	0.438	0.497	0.364	0.439	0.508	0.490
Cr	0.001	0.001	0.001	0.001	0.002	0.002	0.001	0.001	0.000
Fe^{2+}	0.138	0.089	0.101	0.150	0.088	0.059	0.141	0.121	0.143
Mn	0.001	0.001	0.001	0.001	0.001	0.000	0.001	0.001	0.001
Mg	0.421	0.424	0.505	0.462	0.460	0.633	0.480	0.431	0.447
Ni	0.000	0.000	0.001	0.001	0.000	0.001	0.000	0.000	0.001
Zn	0.001	0.001	0.001	0.001	0.001	0.000	0.001	0.001	0.001
Ca	0.496	0.501	0.577	0.548	0.553	0.675	0.566	0.477	0.542
Na	0.478	0.459	0.380	0.431	0.417	0.288	0.405	0.478	0.419
K	0.000	0.000	0.000	0.000	0.000	0.000	0.000	0.000	0.000
Total	4.008	3.994	3.994	4.015	3.988	3.990	4.009	4.002	4.004
Mg#	0.75	0.83	0.83	0.76	0.84	0.91	0.77	0.78	0.76
End-members									
$CaTiAl_2O_6$	0.006	0.006	0.005	0.005	0.004	0.002	0.005	0.006	0.009
$NaCrSi_2O_6$	0.001	0.001	0.001	0.001	0.002	0.002	0.001	0.001	0.000
$NaAlSi_2O_6$	0.470	0.458	0.379	0.425	0.416	0.286	0.404	0.477	0.419
$CaAl_2SiO_6$	0.001	0.047	0.036	0.001	0.037	0.037	0.013	0.010	0.026
$CaFeSi_2O_6$	0.121	0.078	0.089	0.132	0.082	0.055	0.124	0.101	0.123
$CaMgSi_2O_6$	0.367	0.370	0.446	0.408	0.429	0.581	0.423	0.360	0.383
$CaMnSi_2O_6$	0.001	0.001	0.001	0.001	0.001	0.000	0.001	0.001	0.001
$Fe_2Si_2O_6$	0.007	0.005	0.006	0.005	0.003	0.002	0.006	0.009	0.008
$Mg_2Si_2O_6$	0.022	0.026	0.029	0.015	0.016	0.026	0.019	0.031	0.026
$Mn_2Si_2O_6$	0.000	0.000	0.000	0.000	0.000	0.000	0.000	0.000	0.000
Total	0.997	0.992	0.992	0.993	0.990	0.991	0.996	0.996	0.995

(Continues)

TABLE 2 (Continued)

Sample	15	33.1a	38	40	27	129	Fa	Mt	Ok	Ws
Unit	EG 2	EG 2	EG 2	EG 2	EG 3	EG 3	FG	FG	FG	FG
N	30	38	30	25	30	14	30	14	24	15
SiO_2	55.60	56.61	56.23	55.89	55.96	56.29	55.36	56.05	55.53	55.52
TiO_2	0.06	0.08	0.08	0.12	0.05	0.05	0.08	0.11	0.11	0.07
Al_2O_3	9.15	11.29	9.63	11.44	10.01	11.50	8.48	11.03	9.42	6.45
Cr_2O_3	0.08	0.02	0.06	0.02	0.01	0.06	0.05	0.11	0.24	0.05
FeO	1.45	1.64	3.50	3.22	3.49	1.73	5.39	2.40	2.00	1.38
MnO	0.02	0.03	0.03	0.03	0.02	0.02	0.02	0.02	0.02	0.01
MgO	11.59	9.63	10.01	9.16	9.28	9.46	9.65	9.56	11.13	13.71
NiO	0.05	0.02	0.02	0.02	0.02	0.03	0.02	0.03	0.02	0.01
ZnO	0.03	0.03	0.03	0.03	0.02	0.02	0.04	0.04	0.04	0.02
CaO	16.66	14.59	15.53	13.83	14.43	13.71	15.17	14.82	16.74	19.94
Na_2O	4.74	5.65	5.65	6.36	6.59	6.31	5.38	6.12	4.75	3.14
K_2O	0.01	0.01	0.00	0.01	0.00	0.00	0.00	0.00	0.00	0.00
Total	99.44	99.60	100.77	100.13	99.88	99.18	99.64	100.29	100.00	100.32
Si	1.979	1.995	1.988	1.977	1.994	1.993	1.997	1.978	1.971	1.975
Ti	0.002	0.002	0.002	0.003	0.001	0.001	0.002	0.003	0.003	0.002
Al	0.384	0.469	0.401	0.477	0.420	0.480	0.360	0.459	0.394	0.270
Cr	0.002	0.000	0.002	0.001	0.000	0.002	0.001	0.003	0.007	0.001
Fe^{2+}	0.043	0.048	0.103	0.095	0.104	0.051	0.163	0.071	0.059	0.041
Mn	0.001	0.001	0.001	0.001	0.001	0.001	0.001	0.000	0.001	0.000
Mg	0.615	0.506	0.528	0.483	0.493	0.499	0.519	0.503	0.589	0.727
Ni	0.001	0.000	0.000	0.001	0.000	0.001	0.001	0.001	0.001	0.000
Zn	0.001	0.001	0.001	0.001	0.001	0.001	0.001	0.001	0.001	0.000
Ca	0.635	0.551	0.588	0.524	0.551	0.520	0.586	0.560	0.637	0.760
Na	0.327	0.386	0.387	0.436	0.456	0.433	0.376	0.418	0.327	0.217
K	0.000	0.000	0.000	0.000	0.000	0.000	0.000	0.000	0.000	0.000
Total	3.990	3.959	4.001	3.999	4.021	3.982	4.007	3.997	3.990	3.993
Mg#	0.93	0.91	0.84	0.84	0.83	0.91	0.76	0.88	0.91	0.95
End-members										
$CaTiAl_2O_6$	0.002	0.002	0.002	0.003	0.001	0.001	0.002	0.003	0.003	0.002
$NaCrSi_2O_6$	0.002	0.000	0.002	0.001	0.000	0.002	0.001	0.003	0.007	0.001
$NaAlSi_2O_6$	0.325	0.386	0.385	0.436	0.418	0.431	0.356	0.415	0.320	0.215
$CaAl_2SiO_6$	0.028	0.040	0.006	0.018	0.000	0.023	0.000	0.019	0.034	0.026
$CaFeSi_2O_6$	0.040	0.044	0.095	0.083	0.096	0.046	0.139	0.066	0.055	0.039
$CaMgSi_2O_6$	0.566	0.464	0.485	0.420	0.453	0.449	0.444	0.472	0.545	0.693
$CaMnSi_2O_6$	0.000	0.001	0.001	0.001	0.001	0.001	0.001	0.000	0.001	0.000
$Fe_2Si_2O_6$	0.002	0.002	0.004	0.006	0.004	0.003	0.011	0.002	0.002	0.001
$Mg_2Si_2O_6$	0.024	0.021	0.018	0.030	0.019	0.025	0.036	0.013	0.022	0.017
$Mn_2Si_2O_6$	0.000	0.000	0.000	0.000	0.000	0.000	0.000	0.000	0.000	0.000
Total	0.989	0.960	0.998	0.998	0.992	0.981	0.990	0.993	0.989	0.994

Note: Oxides in wt%, cations on the basis of 6 oxygen. All iron is treated as Fe^{2+}. For standard deviations, see Table S1.
Abbreviation: *N*, number of analyses.

TABLE 3 Trace element concentration of omphacite (sample averages) determined by LA-ICP-MS analysis

Sample	4	6	10.3	Vo	St11	St75	113	44	33.1a	38	40	129	Fa	Mt	Ok	Ws
Unit	EG	EG 1	EG 1	EG 1	EG 1	EG 1	EG 1	EG 1	EG 2	EG 2	EG 2	EG 3	FG	FG	FG	FG
N	10	9	12	8	12	10	8	8	9	8	11	10	9	9	8	9
Li	95	131	27	22	53	50	23	259	38	69	41	29	52	36	14	25
Be	1.4	2.2	1.2	0.91	1.0	0.77	0.91	2.3	1.1	1.4	0.79	1.2	0.99	0.97	0.67	0.56
P	29	29	34	30	32	31	26	28	20	35	20	37	19	25	23	26
K	17	17	21	35	17	294	18	23	34	15	11	3,361	11	9.0	19	13
Sc	24	21	23	25	37	16	23	25	32	31	26	18	31	24	16	18
Ti	1,112	1,065	841	1,123	972	668	1,034	994	464	470	584	435	441	598	560	381
V	638	458	484	567	493	362	641	727	297	505	516	302	600	377	271	329
Cr	108	240	384	238	491	423	151	232	80	511	149	234	189	1,258	2,343	468
Mn	264	175	362	277	691	137	214	256	151	132	182	1,912	135	141	122	100
Co	20	12	33	29	17	30	28	10	10	33	26	27	41	18	23	11
Ni	38	13	193	85	14	255	90	8.8	6.1	109	67	34	174	130	89	5.2
Cu	0.75	0.76	3.5	0.56	0.97	2.8	0.84	0.72	0.92	1.5	0.62	0.97	1.3	1.1	1.5	bdl
Zn	194	130	96	126	124	55	120	177	61	152	120	406	139	90	70	46
Ga	33	27	21	27	24	19	26	32	20	26	25	18	25	22	19	13
Ge	1.0	0.95	0.93	0.97	1.1	1.4	1.0	1.1	0.97	0.98	1.1	1.4	0.84	0.81	0.81	1.1
Sr	158	75	146	154	94	79	133	141	72	65	39	95	34	35	103	102
Y	2.0	0.96	3.5	1.3	16	0.62	1.0	2.2	0.29	0.56	0.68	25	0.55	0.75	0.40	0.39
Zr	13	9.1	9.5	14	7.4	5.5	9.5	11	1.8	2.2	3.4	1.9	2.7	3.5	3.6	2.6
Nb	0.025	0.030	0.010	0.012	0.034	0.0077	0.011	bdl	0.052	0.0088	0.018	0.029	bdl	0.037	0.021	0.027
Sn	3.4	2.8	1.0	1.0	1.4	1.2	1.1	4.5	0.83	1.1	1.0	6.5	0.77	0.81	0.55	0.35
Ba	0.11	0.18	0.11	0.11	0.15	0.69	0.12	0.23	0.14	0.29	0.39	6.0	0.12	0.16	0.17	0.20
La	0.66	0.21	0.19	0.57	0.046	0.068	0.36	0.97	0.025	0.033	0.028	0.026	0.0059	0.036	0.014	bdl
Ce	3.9	1.4	1.5	3.4	0.20	0.50	2.2	4.9	0.055	0.15	0.20	0.11	0.014	0.035	0.023	0.016
Pr	0.96	0.36	0.48	0.76	0.073	0.16	0.52	1.0	0.033	0.067	0.075	0.056	bdl	0.016	0.015	0.016
Nd	6.3	2.7	3.5	5.1	0.93	1.5	3.8	6.5	0.18	0.58	0.65	0.57	0.057	0.17	0.089	0.053
Sm	2.4	1.0	1.6	1.4	1.1	0.86	1.1	2.3	0.14	0.32	0.64	0.61	bdl	0.14	0.12	0.055
Eu	0.60	0.25	0.47	0.40	0.57	0.27	0.25	0.64	0.053	0.12	0.19	0.31	0.035	0.059	0.056	0.032
Gd	1.5	0.69	1.1	1.0	2.2	0.52	0.73	1.6	0.20	0.35	0.50	1.8	0.19	0.30	0.17	bdl
Tb	0.16	0.078	0.14	0.11	0.44	0.056	0.082	0.17	0.030	0.050	0.061	0.45	0.038	0.047	0.029	0.017
Dy	0.67	0.31	0.80	0.45	3.0	0.24	0.31	0.71	0.14	0.23	0.27	4.0	0.15	0.24	0.13	0.11

(Continues)

TABLE 3 (Continued)

Sample	4	6	10.3	Vo	St11	St75	113	44	33.1a	38	40	129	Fa	Mt	Ok	Ws
Unit	EG	EG 1	EG 1	EG 1	EG 1	EG 1	EG 1	EG 1	EG 2	EG 2	EG 2	EG 3	FG	FG	FG	FG
N	10	9	12	8	12	10	8	8	9	8	11	10	9	9	8	9
Ho	0.082	0.042	0.14	0.057	0.67	0.032	0.045	0.089	0.013	0.032	0.034	1.0	0.029	0.035	0.019	0.022
Er	0.15	0.077	0.47	0.12	1.9	0.060	0.098	0.18	0.048	0.064	0.063	5.4	0.067	0.071	0.052	0.040
Tm	0.020	0.016	0.21	0.012	0.77	0.012	0.016	0.021	0.011	0.015	0.0079	1.7	0.018	0.018	0.012	0.0022
Yb	0.097	0.098	0.72	0.079	3.6	0.067	0.081	0.091	bdl	0.098	0.056	12	0.15	0.065	0.030	bdl
Lu	0.016	bdl	0.12	0.021	1.0	0.012	bdl	0.017	bdl	0.017	0.0088	1.7	0.035	0.0089	0.0070	0.0065
Hf	0.80	0.54	0.55	0.86	0.48	0.37	0.61	0.72	0.18	0.21	0.24	0.13	0.31	0.31	0.23	0.20
W	0.023	0.047	0.038	0.040	0.072	0.11	0.048	0.021	0.068	bdl	0.045	11	0.076	bdl	0.045	0.11
Pb	2.0	1.5	2.5	1.7	0.46	2.8	2.0	9.4	0.53	0.98	0.54	7.8	0.18	0.45	0.40	0.43

Note: Element concentrations are given in ppm. For standard deviations, see Table S2.
Abbreviations: bdl, below detection limit; *N*, number of analyses.

the physical principles, a greater analytical error (Kovács et al., 2008; Sambridge et al., 2008). By choosing a sample thickness of less than 0.25 mm, the maximum of the measured absorbances (not normalized) could be limited, so that the uncertainty does not exceed 10% (see fig. S1 in Sambridge et al., 2008).

The integral absorbance was determined by fitting the spectra between 3,000 and 3,700 cm^{-1}. For baseline correction, a third degree polynomial was used, which adequately matches the H_2O-free regions of the spectra. The peak fit was obtained by a combination of Lorentzian and Gaussian functions applying a peak-fit software. The width of peaks in the region 3,270–3,370 cm^{-1}, with mostly flat shoulders, was constrained to 200 cm^{-1}. The total amount of H_2O in omphacite (Table 4), including structural hydroxyl and possibly present molecular water, was determined from the absorption of bands with maxima in the wavenumber range 3,000–3,700 cm^{-1}. Additionally, the band-specific H_2O contents (Table 4) were determined for the four bands recorded by fitting the spectra in the following wavenumber range: band II, centred at 3,455 ± 10 cm^{-1}: 3,400–3,500 cm^{-1}; band III, centred at 3,522 ± 10 cm^{-1}: 3,500–3,550 cm^{-1}; band I, centred between 3,270 and 3,370 cm^{-1}: 2,900–3,400 cm^{-1}; band IV, centred at 3,611–3,635 cm^{-1}: 3,550–3,700 cm^{-1}. The H_2O contents were calculated by applying the mineral-specific molar absorption coefficient of Bell et al. (1995) because the same approach was previously applied for garnet from the same samples (Gose & Schmädicke, 2018). The uncertainty due to the calibration is 4.4% (Bell et al., 1995). Because omphacite analysed in this study contains more Al and Na but less Mg and Fe, the systematic uncertainty due to calibration is 10–20%. Additional uncertainty is caused by spectra fitting so that the total uncertainty of the calculated H_2O contents given in Table 4 may well be 30%. For better comparison with literature data, total H_2O contents were also determined using the calibration of Libowitzky and Rossman (1997).

5 | RESULTS

5.1 | Major and trace element composition

Comparing all investigated samples, the major and trace element composition of omphacite is variable (Tables 2 and 3; Figure 2). By contrast, grains from a single sample show fairly constant composition without any zonation. The Mg/(Mg+Fe) ratios (Mg#) cover a range from 0.75 to 0.95 (Table 2) and negatively correlate with TiO_2 ($r = -0.70$; Figure 2). Dark eclogite has generally lower

TABLE 4 Content of structural water in eclogitic omphacite from Erzgebirge (EG) and Fichtelgebirge (FG)

Sample	Grains/ spectra	H_2O (ppm) band II	H_2O (%) band II	H_2O (ppm) band III	H_2O (%) band III	H_2O (ppm) band I	H_2O (%) band I	H_2O (ppm) band IV	H_2O (%) band IV	H_2O (ppm) bands I–IV	H_2O (ppm) bands II + III	H_2O (ppm) bands II + III + IV	H_2O (ppm) Grt	K_D Grt/Omp bands I–IV	K_D Grt/Omp bands II + III + IV	H_2O* (ppm) bands I–IV
4	14/22	414	74	45	8	66	12	33	6	558	459	**492**	43	0.08	0.09	290
6	14/22	699	73	30	3	123	13	108	11	960	729	**837**	85	0.09	0.10	519
10.3	14/23	963	74	135	10	159	12	42	3	1,299	1,098	**1,140**	60	0.05	0.05	683
Vo[a]	72/72	774	74	111	11	135	13	27	3	1,047	885	**912**	81	0.08	0.09	531
St11	20/20	711	78	48	5	123	14	24	3	906	759	**783**	164	0.18	0.21	477
St75	23/28	339	58	111	19	87	15	48	8	585	450	**498**	40	0.07	0.08	314
113	18/20	594	66	135	15	108	12	54	6	891	729	**783**	84	0.09	0.11	479
44	18/23	618	65	9	1	255	27	69	7	951	627	**696**	-	-	-	428
46a	12/12	717	66	48	4	171	16	150	14	1,086	765	**915**	61	0.06	0.07	585
Avg EG Unit 1		*654*	*69*	*85*	*9*	*137*	*15*	*67*	*7*	*944*	*739*	***806***	*78*	*0.09*	*0.10*	*478*
15	26/26	582	63	78	8	180	19	84	9	924	660	**744**	17	0.02	0.02	465
33.1a	20/20	420	69	60	10	72	12	63	10	615	480	**543**	12	0.02	0.02	317
38	27/27	420	72	18	3	117	20	27	5	582	438	**465**	160	0.27	0.34	276
40	20/29	690	72	108	11	102	11	54	6	954	798	**852**	-	-	-	497
Avg EG Unit 2		*528*	*69*	*66*	*8*	*118*	*16*	*57*	*8*	*769*	*594*	***651***	*63*	*0.10*	*0.13*	*389*
27	22/22	522	49	36	3	210	20	294	28	1,062	558	**852**	28	0.03	0.03	574
129	23/25	438	61	15	2	132	18	135	19	720	453	**588**	-	-	-	366
Avg EG Unit 3		*480*	*55*	*26*	*3*	*171*	*19*	*215*	*23*	*891*	*506*	***720***	*28*	*0.03*	*0.03*	*470*
Fa	24/28	432	63	90	13	132	19	24	4	678	522	**546**	15	0.02	0.03	337
Mt	22/24	858	71	186	15	120	10	45	4	1,209	1,044	**1,089**	13	0.01	0.01	630
Ok	23/26	660	66	132	13	129	13	72	7	993	792	**864**	20	0.02	0.02	534
Ws	23/25	453	46	234	24	162	17	123	13	972	687	**810**	8	0.01	0.01	552
Avg FG		*601*	*62*	*161*	*16*	*136*	*15*	*66*	*7*	*963*	*761*	***827***	*14*	*0.01*	*0.02*	*513*

Note: The H_2O data for garnet are from Gose and Schmädicke (2018). The concentrations for both minerals were calculated with the absorption coefficient of Bell et al. (1995). The total contents for omphacite, derived from the Libowitzky and Rossman (1997) calibration* are shown for comparison. The band-specific water contents are given in ppm and in % of the total water content. The concentrations given for the main bands II and III and for the minor band IV are ascribed to structural H_2O; H_2O contents reflected by band I may include different H_2O sources. See text for further explanation.

[a]Data from three perpendicular thin sections.

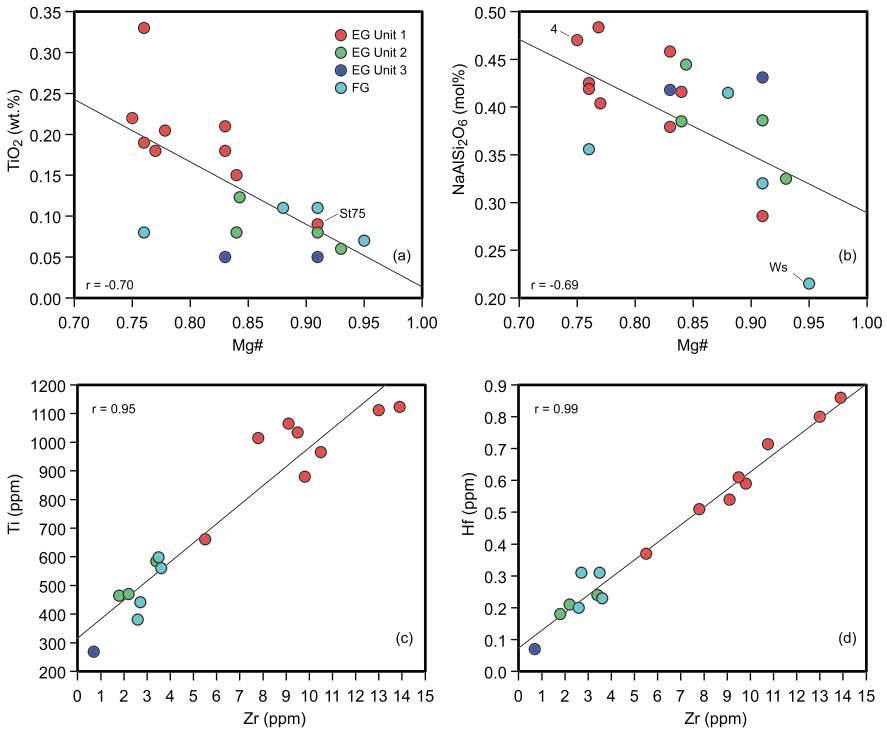

FIGURE 2 Binary scatter diagrams showing the composition of omphacite (sample averages). (a) Mg# versus TiO_2, (b) amount of jadeite component versus Mg#, (c) Ti versus Zr, and (d) Hf versus Zr. Data in (a) and (b) are from microprobe analysis, and data in (c) and (d) from LA-ICP-MS analysis. *r*, correlation coefficient [Colour figure can be viewed at wileyonlinelibrary.com]

Mg# and higher TiO_2 contents than light-coloured eclogite. The jadeite content is highly variable spanning a range between 21.5 and 47.7 mol.% and showing a broad negative correlation with Mg# ($r = -0.69$; Figure 2). The lowest jadeite content (21.5 mol.%) and the highest Mg# (0.95) are observed in the light-coloured sample Ws. Vice versa, sample 4 (dark eclogite) has the lowest Mg# (0.75) and the second highest jadeite content of 47 mol.% (Table 2; Figure 2); only omphacite in sample 44 is slightly richer in jadeite (i.e., 47.7 mol.%). Given cation totals of 3.98–4.02 (except one sample), the amount of the Ca-Eskola component (Schmädicke & Müller, 2000) is either zero or negligible.

Major and minor element composition of omphacite is uncorrelated to the unit, with the exception of TiO_2. This implies that omphacite composition in the studied samples is primarily governed by the bulk rock compositions, in agreement with literature data (Schmädicke, 1994; Schmädicke & Will, 2021). Also, the different Ti contents in omphacite from quartz and coesite eclogite (Figure 2) are ascribed to the bulk rock composition, because quartz eclogite from both EG and FG samples has lower bulk rock TiO_2 contents (range: 0.05–0.12 wt%) than coesite eclogite from EG Unit 1 (range for all samples: 0.09–0.33 wt%; range without sample St75: 0.15–0.33 wt%).

Concerning trace elements, samples from Erzgebirge and Fichtelgebirge differ only in a few elemental concentrations, particularly in Cr (EG: 80–511 ppm; FG: 189–2,343 ppm) and Pb (EG: 0.53–9.4 ppm; FG: 0.18–0.43 ppm) and to a lesser degree in K and Sr (Table 3). Furthermore, omphacite from coesite eclogite has higher contents of Zr, Hf, and light (L) and medium (M) REE compared with quartz eclogite from both EG and FG (Table 3; Figures 2 and 3). Notably, in the Erzgebirge, these elements show equal bulk rock concentrations in both eclogite types (Schmädicke & Will, 2021). The Zr contents of omphacite in coesite eclogite (5.5–14 ppm) do not overlap with those in quartz eclogite (0.7–3.6 ppm). The same applies to Hf and most LREE and MREE, such as Ce (coesite eclogite: 0.2–4.8 ppm, quartz eclogite: ≤0.2 ppm) and Nd (coesite eclogite: 0.65–6.4 ppm; quartz eclogite: 0.05–0.65 ppm). In addition, the Zr content is positively correlated with both Ti ($r = 0.95$) and Hf ($r = 0.99$; Figure 2). The normalized REE concentrations of quartz eclogite are generally lower than in primitive mantle (PM), in many cases even <0.1 relative to PM, whereas the LREE and MREE contents of most coesite eclogite samples exceed the PM values and lie in the range of 1–10 times that of PM (Figure 3).

5.2 | IR spectra

All analysed grains show IR absorption bands in the range of 3,200–3,650 cm^{-1} (Figure 4), indicative of structural H_2O in pyroxene (Skogby, 2006; Skogby et al., 1990; Stalder & Ludwig, 2007). Four bands (or band groups) can be distinguished, centred at 3,270–3,370 cm^{-1} (band I), at 3,455 ± 10 cm^{-1} (band II), at 3,522 cm^{-1} (III), and

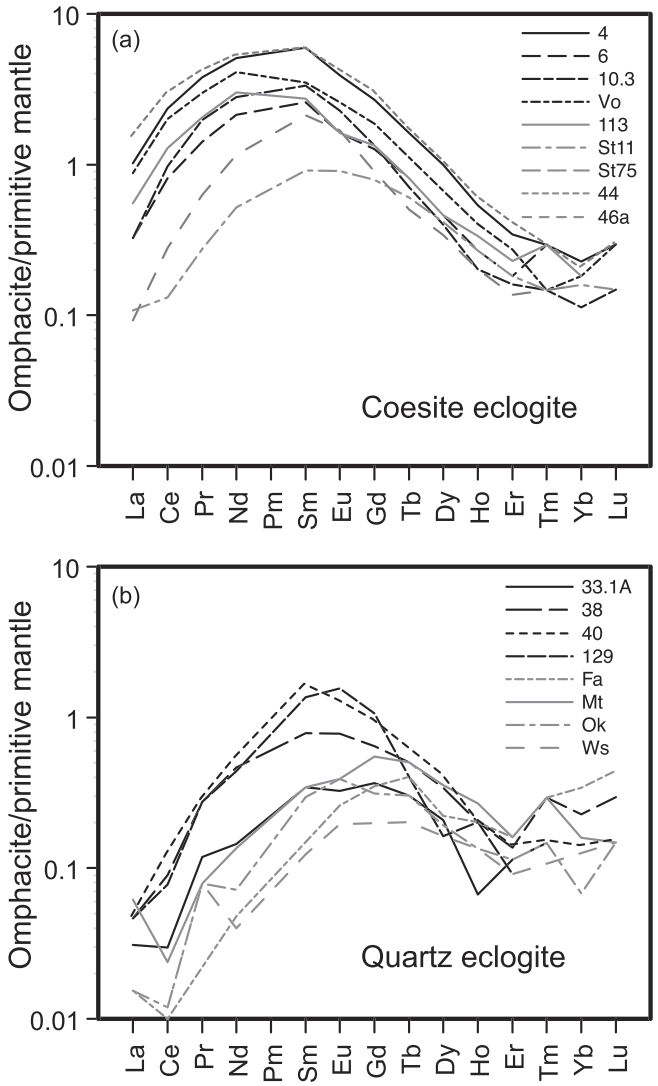

FIGURE 3 REE patterns for omphacite using sample averages, normalized to the values for primitive mantle by McDonough and Sun (1995). (a) Coesite eclogite samples from EG Unit 1; (b) quartz eclogite from EG Units II (33.1a, 38, 40) and III (129) and FG (Fa, Mt, Ok, Ws)

at 3,611–3,635 cm^{-1} (IV). Bands II and III are strong and relatively sharp in all samples, whereas the broad band I and the sharp band IV are much weaker. All four bands were reported from clinopyroxene, but only bands II, III, and IV were found in omphacite (e.g., Skogby, 2006; Skogby et al., 2016). In some cases, omphacite reveals only bands II and III (Katayama et al., 2006; Koch-Müller et al., 2004).

The intensity of bands II and III strongly varies between different omphacite grains per sample (Figure 5) but is constant in different volumes of a single grain, such as grain cores and rims. The inter-grain scattering is related to different grain orientation and indicates pronounced pleochroic behaviour of the two prominent bands. From Figure 5, it is obvious that the grains are randomly oriented. In addition, the relative peak height of bands II and III is also variable (Figures 4 and 5). In most samples, band II is larger than band III, but there are also a few samples in which the two bands have equal height (Fa, Ok) or in which band III is the larger one (St75, Ws). The latter two samples are characterized by omphacite with the lowest jadeite (21.5 and 28.6 mol.%) and the highest diopside content (69.3 and 58.1 mol.%) of the sample set, and omphacite from samples Fa and Ok is also relatively poor in jadeite (35.6 and 32.0 mol.%). Band II is known to be the most intense one in omphacite but not in diopside (e.g., Skogby, 2006). Thus, its intensity seems to be related to jadeite content, which well agrees with our data.

In many samples, the intensity of the generally small band IV is usually more or less uniform indicating less pronounced pleochroism. In other samples (6, 46a, St75, 15, 33.1, 27, 129, Ok, and Ws), band IV has strongly varying intensity. Moreover, if the spectra from a single sample are compared, it is obvious that this variation is not continuous because the band is either small (in most cases) or strongly enhanced (for examples, see Figure 5). In some of the spectra recorded for samples St75, 15, 27, and Ws, band IV is the strongest band, even exceeding the peak height of bands II and III.

Additional bands at higher wavenumber (i.e., 3,670–3,700 cm^{-1}), indicative of secondary amphibole (Skogby et al., 1990), are restricted to samples Fa, 15, 38, 40, and 44, where they occur only in very few (1–3) of the recorded spectra.

5.3 | H_2O content

At this stage, it is not clear if bands I and IV are due to structural hydroxyl (with concentrations given as wt.-ppm H_2O) in omphacite (see previous section and Section 6). Accordingly, the H_2O content related to every single band is given separately, and the total H_2O content of each sample was determined by summing the data of all bands (i.e., I–IV), of only bands II + III, and of bands II + III + IV, respectively (Table 4). For the calculation of H_2O contents, the outlier spectra with extremely large bands of type IV were excluded because these spectra involve H_2O species from another source (see below). Band II accounts for the largest part of H_2O in all samples (i.e., 46–78%), also including the two samples (St75, Ws) in which band II has lower height than band III. The H_2O content related to band III (1–24%) is similar to that of bands I (10–27%) and IV (3–28%).

The total H_2O contents in the sample set (Table 4), calculated from bands I–IV, range from 558 to

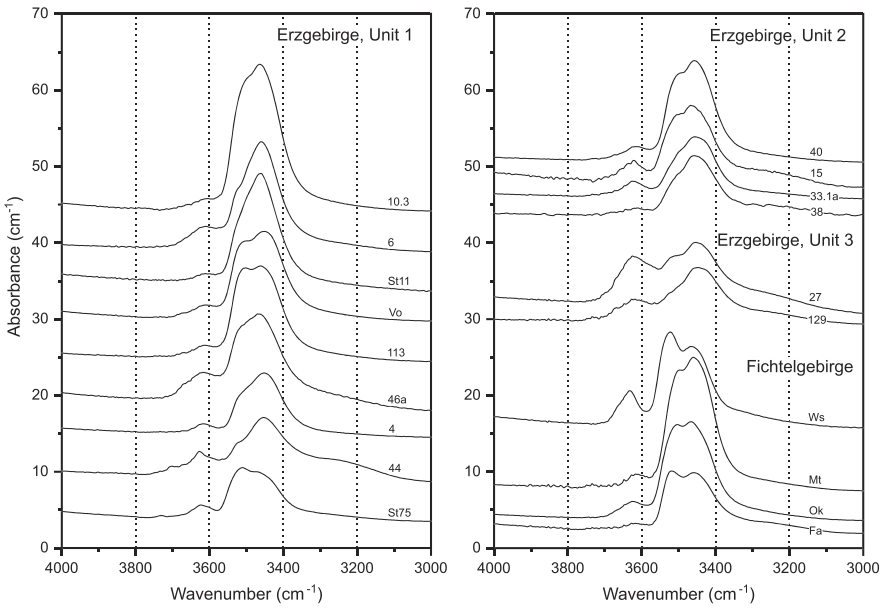

FIGURE 4 IR absorption spectra of omphacite. (a) Eclogite from Erzgebirge Unit 1; (b) Eclogite from EG Units 2 and 3 and Fichtelgebirge. The spectra are sample averages and are normalized to 1 cm sample thickness

1,299 ppm using the calibration of Bell et al. (1995). Values derived with the formula by Libowitzky and Rossman (1997) for better comparison with literature data (see below) are ~50% lower (Table 4). Differences in H_2O are neither observed between quartz and coesite eclogite nor between EG and FG samples. Including only bands II, III, and IV, the total contents are somewhat lower (492–1,140 ppm), but a relation to either eclogite type or unit is not visible either. The same applies to H_2O contents based on bands II and III (459–1,098 ppm). No matter which of the three different totals is used, a correlation of omphacite data with previously determined H_2O in garnet is not observed (Table 4). As a result, the K_D for H_2O partition between garnet and omphacite scatter over 1 order of magnitude, for example, 0.01–0.27 (including omphacite bands I–IV) and 0.01–0.34 (including bands II + III + IV; Table 4). However, if samples 38 and St11 with unusually H_2O-rich garnet are excluded, the range for K_D is smaller (i.e., 0.01–0.09 for bands I–IV; 0.01–0.11 for bands II + III + IV). Neglecting outlier samples, the typical K_D for quartz eclogite (0.01–0.03) is distinctly lower than that for coesite eclogite (0.08–0.11).

6 | DISCUSSION AND CONCLUSIONS

6.1 | Relation between H_2O content and other parameters

The total H_2O content derived from bands I to IV neither correlates with omphacite composition nor with eclogite type or unit, respectively, suggesting that the PT conditions have no first-order control on the H_2O content in omphacite. The opposite has been observed for garnet from the same samples, in which H_2O positively correlates with the Ca and Ti content of garnet. In addition, garnet from coesite eclogite contains significantly more H_2O compared with quartz eclogite (Gose & Schmädicke, 2018); the reason for this is discussed below.

In addition, the present results do not agree with those of previous studies on omphacite, which showed that the mineral's H_2O content is correlated to pressure (Katayama & Nakashima, 2003; Koch-Müller et al., 2004). However, the previously observed trends are controversial because they involve both positive and negative correlations between H_2O and pressure. Orogenic eclogite from the Kokchetav massif (Katayama & Nakashima, 2003) showed a positive trend because H_2O contents in omphacite increase from quartz to coesite and to diamond eclogite. By contrast, Koch-Müller et al. (2004) found a negative trend for eclogite xenoliths. Moreover, a study on eclogite xenoliths revealed that a relation between H_2O in omphacite and temperature exists, but, again, both positive and negative correlations were reported, depending on the eclogite subtype (Huang et al., 2014).

If the individual IR bands and the related H_2O contents of the present sample set are treated separately, some trends with respect to omphacite composition become obvious. For instance, the H_2O content defined by band II is positively correlated (albeit weakly) to both Ti and tetrahedral Al (Figure 6). However, such a relation is not found for band III. Instead, H_2O due to band III shows a negative correlation with Na (and jadeite

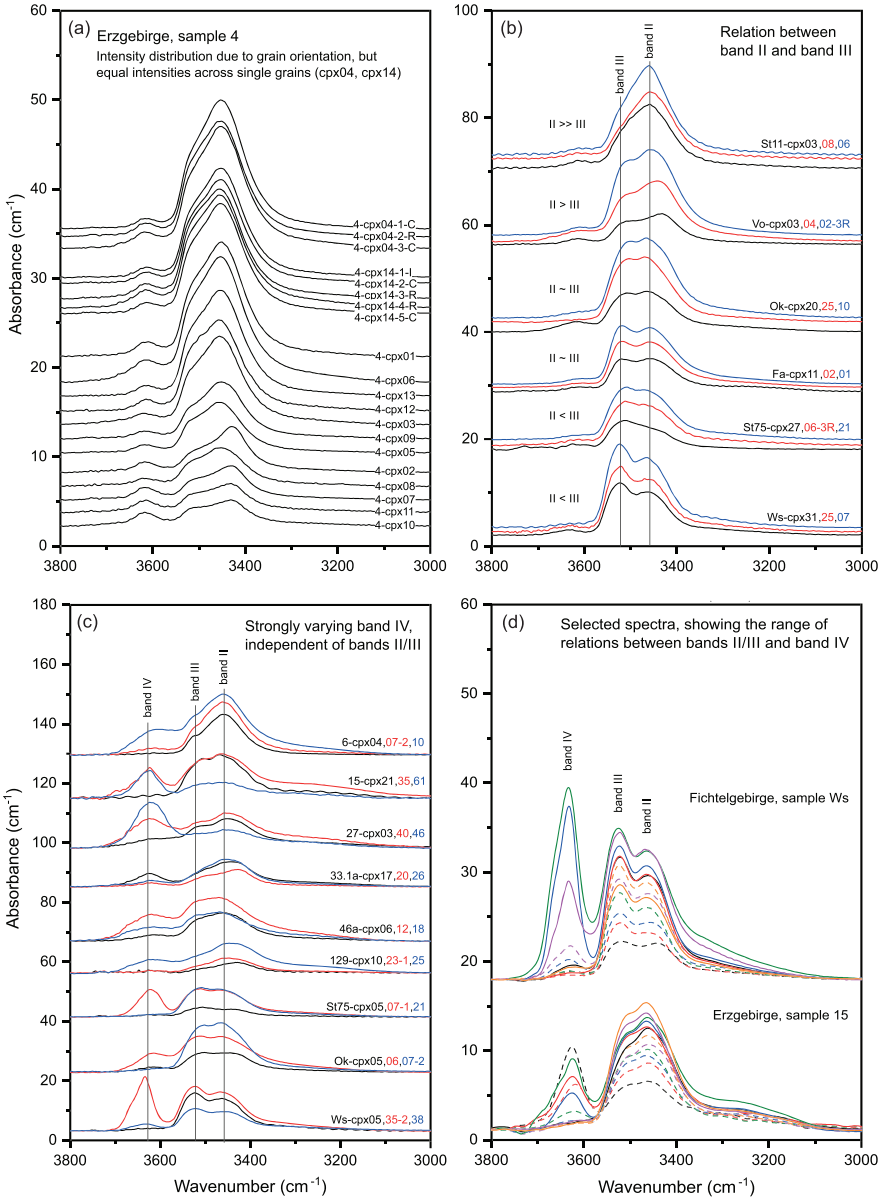

FIGURE 5 IR absorption spectra of individual omphacite grains. (a) Example of variability of spectra in a single sample; (b) relative intensities of bands II and III and pleochroic behaviour of selected samples from Erzgebirge and Fichtelgebirge. The three orthogonal directions are illustrated in black, blue, and red; (c) examples of omphacite grains with variable type IV bands in three different directions per sample; (d) variability of spectra in different grains of samples Ws and 15 illustrating the variability of relative band intensities. All spectra are normalized to 1 cm sample thickness [Colour figure can be viewed at wileyonlinelibrary.com]

content) and a positive one with Ca (and diopside content) but, in turn, no correlation with Ti and tetrahedral Al (Figure 7). By contrast, bands I and IV are not related to any compositional variable.

Furthermore, the H_2O content of garnet in the same samples depends (i) on the Ca content of garnet and (ii) on the co-stability of hydrous minerals in the peak assemblage. The Ca-rich garnet in coesite eclogite hosts considerably more H_2O compared with the Ca-poor garnet in quartz eclogite, which contains little or no H_2O (Gose & Schmädicke, 2018). Given this obvious relation, the authors argued that the co-stability of hydrous minerals may be even more important in this context. As long as zoisite, calcic amphibole, and ±phengite are present, as in quartz eclogite, garnet takes up little H_2O. In coesite eclogite, where garnet coexists with a 'dry' peak assemblage, it incorporates considerably more H_2O. This relation was confirmed by an exceptional coesite eclogite with peak-metamorphic phlogopite (St75) because garnet in this sample is as poor in H_2O as garnet in quartz eclogite. For omphacite, a relation between H_2O and the co-stability of hydrous minerals is not obvious, with the exception of the phlogopite-bearing sample, because omphacite in this rock is equally H_2O poor as garnet. The latter result—based on an exotic sample—is difficult to verify by further studies due to the lack of peak-metamorphic phlogopite in common orogenic eclogite. Nevertheless, a relation between H_2O in NAMs and the presence or absence of hydrous minerals was not only suggested for garnet (Gose & Schmädicke, 2018) but also for olivine (Kang et al., 2017) and may be valid for omphacite.

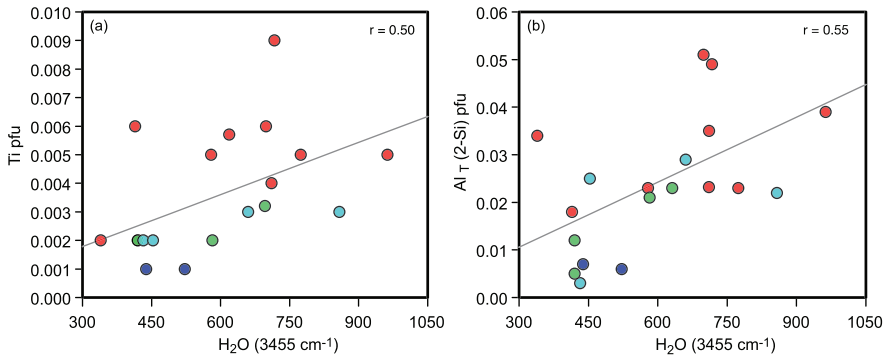

FIGURE 6 Binary scatter diagrams showing the relation between the water content deduced from band II (3,455 cm^{-1}) and the contents of Ti (a) and tetrahedral Al (b) per formula unit and the same for band III (3,522 cm^{-1}; Table 4) relative to Ti (c) and Al (d), respectively. *r*, correlation coefficient [Colour figure can be viewed at wileyonlinelibrary.com]

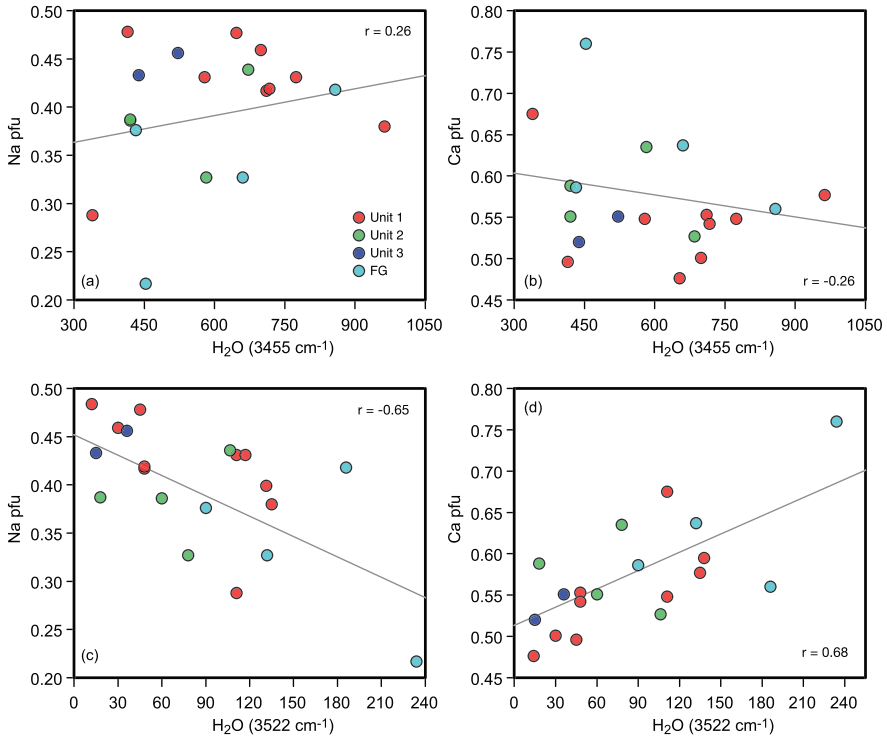

FIGURE 7 Binary scatter diagrams showing the water contents deduced from band II (3,455 cm^{-1}) in relation to Na (a) and Ca (b) per formula unit and water due to band III (3,522 cm^{-1}; Table 4) relative to Na (c) and Ca (d). *r*, correlation coefficient [Colour figure can be viewed at wileyonlinelibrary.com]

The new results on orogenic eclogite imply that omphacite and garnet, concerning H_2O incorporation, behave differently with respect to PT conditions. Hence, the difference in K_D between quartz and coesite eclogite (see above) is primarily due to different H_2O contents of garnet.

6.2 | IR band assignment

The IR bands II and III recorded in this study are typical for omphacite from both eclogite xenoliths (Huang et al., 2014; Koch-Müller et al., 2004) and orogenic eclogite (Katayama et al., 2006; Katayama &

Nakashima, 2003; Konzett et al., 2008; Skogby et al., 2016). Band II commonly occurs also in diopside, but band III is only observed at low SiO_2 activity (Purwin et al., 2009; Stalder & Ludwig, 2007). The band near 3,455 cm^{-1} (our type II) was reported to be the strongest one in omphacite and related to vacancies on the M2 site (Koch-Müller et al., 2004; Libowitzky & Beran, 2006; Smyth et al., 1991). The same interpretation was given for diopside (Purwin et al., 2009; Stalder & Ludwig, 2007). Band III (at ~3,522 cm^{-1}) was attributed to tetrahedral Al (Koch-Müller et al., 2004). However, our data suggest a different interpretation, because band II (but not band III) correlates with tetrahedral Al in the present samples (Figure 6). The intensity of band III, on the other hand, shows a positive correlation with diopside (or Ca) content and a negative one with jadeite (or Na; Figure 7). In fact, Bromiley and Keppler (2004) suggested up to six H substitution mechanisms for Na-bearing pyroxene, three of them are related to the band ~3,520 cm^{-1}. Judging from our data, we conclude that the incorporation of H in omphacite may, indeed, be facilitated by tetrahedral Al, but this substitution may be reflected by band II rather than band III. If true, the H substitution mechanism, causing band III, is uncertain.

The possibility that low H_2O activity favours bands with lower wavenumber (Patkó et al., 2019) does not explain the variation of the relative intensities of bands II and III (3,455 and 3,520 cm^{-1}) observed in this study. This is because the exceptional samples with the largest type III bands (St75, Ws) or with equally large type II and III bands (Fa, Ok) do not contain more H_2O than samples with band II > band III. The finding that relatively large type III bands occur in specimens with low jadeite content indicates that, in the present case, the relative band intensities are simply governed by omphacite composition.

In addition, a band at ~3,620 cm^{-1} (our type IV) is not uncommon for omphacite; however, this band is not always present and its assignment is controversial (Huang et al., 2014; Koch-Müller et al., 2004; Konzett et al., 2008). In most cases, this band is due to structural H_2O in omphacite (Huang et al., 2014; Skogby et al., 2016) supported by the observation that such a band is the most intense one in augite (Bell et al., 1995; Skogby et al., 1990) and probably caused by vacancies on the M2 site (e.g., Bromiley & Keppler, 2004). By contrast, Koch-Müller et al. (2004) ascribed this band solely to included sheet silicates of the chlorite group and did not consider it for the calculation of H_2O contents in omphacite.

In our sample set, the observed behaviour of band IV (see Section 5) indicates structural H_2O in omphacite in most (or all) samples and, in some cases, additional water due to inclusions of a hydrous mineral causing IR absorption in the same wavenumber range. In the case that band IV has uniform intensity in all or most spectra of a sample, the band is ascribed to structural H_2O in omphacite. In such cases, the contribution of this band to the overall H_2O content is relatively small (i.e., 3–14%), depending on the sample. By contrast, the few outlier spectra with considerably stronger type IV bands, compared with the majority of spectra recorded for the same grain, are ascribed to phengite inclusions (e.g., Figure 5). This is supported by a TEM study (Schmädicke & Müller, 2000) on one of the four eclogite samples, in which the intensity of band IV partially exceeds that of band II. For this sample (St75), it was shown that omphacite hosts narrow lamellae (≤0.15 μm width) of phengite, which were interpreted as an exsolution phenomenon due to cooling and decompression (Schmädicke & Müller, 2000). Based on this former study and the observation that phengite has a sharp, intense band at 3,620–3,630 cm^{-1} (see Figure S1), we interpret the outlier spectra of samples St75, 15, and Ok showing an over-pronounced type IV band in terms of submicroscopic phengite lamellae. The same possibly applies to some of the spectra collected for samples 6, 46a, and 33.1a. In the case of samples 27 and 129, the situation is different because relatively intense type IV bands are a common feature and present in most of the recorded spectra. This may be due to the numerous prograde inclusions of hydrous minerals that are very typical for the extremely fine-grained eclogite samples from EG Unit 3.

Notably, the spectrum of phengite (Figure S1) displays an additional broad IR absorption band (or a group of bands) near 3,300 cm^{-1}, which is indistinguishable from band I in omphacite. Therefore, it is possible that also band I, like band IV, includes different H_2O species, namely, structural H_2O in omphacite and H_2O from phengite inclusions. This notion is supported by literature examples showing a correlation between bands I and IV. For instance, a strong type IV band was found in only six from several hundred omphacite spectra, and in these six cases, an additional band near 3,300 cm^{-1} (our type I) occurred (Huang et al., 2014). However, if we compare the intensities of bands I and IV in our samples, no correlation is visible. This does not exclude the possibility that band I is (partly) related to submicroscopic phengite, but it implies an additional source contributing to this band. One possibility is structural H_2O in omphacite. However, a band ~3,300 cm^{-1} rarely occurs in clinopyroxene but is very common in orthopyroxene (e.g., Gose & Schmädicke, 2021; Stalder et al., 2015). In clinopyroxene, it is known from diopside and Na-rich pyroxene (Bromiley & Keppler, 2004; Purwin et al., 2009; Skogby

et al., 1990). Although the related OH incorporation mechanism is unknown, the substitution $Si^{4+} = Al^{3+} + H^{+}$ could be a possibility because the latter is known to cause absorption bands at 3,310–3,380 cm^{-1} in quartz (Stalder, 2021). The other possibility is molecular H_2O in fluid inclusions, as found in numerous spectra of coexisting garnet (Gose & Schmädicke, 2018; Schmädicke & Gose, 2017). However, at the present state of knowledge, the nature of band I remains ambiguous and may be related to structural and molecular H_2O in omphacite and phengite inclusions.

6.3 | 'Real' H_2O contents

Due to the possibility that two of the IR bands may include some water from phengite and/or fluid inclusions, the content of structural H_2O in omphacite needs to be re-evaluated. The values obtained by summing the absorbance from bands I to IV (range: 558–1,299 ppm; Table 4) represent the upper limit for structural H_2O in omphacite, and those derived from only bands II and III define the minimum concentration (range: 438–1,098 ppm). However, because also band IV is attributed to structural H_2O in omphacite, the most realistic result is derived by summing the absorbance due to bands II, III, and IV after excluding the outlier spectra with large type IV bands. Using this approach, the content of structural H_2O is in the range of 465–1,140 ppm. In Erzgebirge samples, omphacite of coesite eclogite has a somewhat higher average content (806 ppm) than that of quartz eclogite from Units 2 (651 ppm) and 3 (720 ppm). Quartz eclogite from Fichtelgebirge yielded the highest average content of 827 ppm H_2O in omphacite, which is very close to the value for EG coesite eclogite. However, these differences are not significant because they do not exceed the analytical uncertainty. Moreover, the ranges of H_2O contents are very similar in all units. Accordingly, the observed difference in H_2O partition between quartz (K_D Grt/Omp = 0.01–0.03) and coesite eclogite (K_D Grt/Omp = 0.08–0.11) is solely due to the variation of H_2O contents in garnet.

Because of the discovered correlations of H_2O with major and minor elements in omphacite and the constant H_2O content on grain scale (see above), the obtained H_2O contents of omphacite are, most probably, a primary feature rather than the result of H_2O loss. The same characteristics were described from coexisting garnet (Gose & Schmädicke, 2018). During decompression, garnet incorporated secondary structural H_2O—providing a very strong argument against decompressional water loss.

The measured H_2O concentrations in omphacite (approximate range: 450–1,150 ppm) compare well with literature data for H_2O in omphacite from both orogenic and xenolithic eclogite. Omphacite of orogenic UHP eclogite from Kokchetav was reported to contain up to 870 ppm (Katayama et al., 2006), and omphacite of quartz eclogite from Saualpe and Pohorje (Alps) hosts 145–580 ppm H_2O (Konzett et al., 2008). Higher H_2O contents in omphacite (530–870 ppm) of eclogite samples from Pohorje were reported by Skogby et al. (2016). For comparing the data for orogenic eclogite obtained in different studies, the analytical details need to be considered. With one exception (Katayama et al., 2006; secondary ion mass spectrometry), all data were obtained by IR spectroscopy. However, the IR studies used different calibration coefficients. For instance, applying the same calibration coefficient as in the present study (Bell et al., 1995) to the Saualpe and Pohorje samples, the H_2O contents would be ~300–1,200 ppm (based on data in Konzett et al., 2008) and 1,000–1,750 ppm (for data in Skogby et al., 2016), respectively. Thus, our data compare very well with those of Kokchetav UHP eclogite and also quartz eclogite samples from the Alps (Konzett et al., 2008) but are lower than the concentrations reported by Skogby et al. (2016). Similar contents as in omphacite of orogenic eclogite were found in xenolithic samples such as omphacite from Udachnaya (i.e., 61–790 ppm; Koch-Müller et al., 2004) and Roberts Victor eclogite xenoliths (i.e., 211–1,496 ppm; Huang et al., 2014).

6.4 | Implications for H_2O storage and transport in eclogite

The present study shows that omphacite of quartz eclogite from two Erzgebirge units (sample averages: 465–852 ppm) and a third one from Fichtelgebirge (546–1,089 pm) contains as much H_2O as omphacite from EG coesite eclogite (492–1,140 ppm). This result implies that the H_2O content in omphacite of orogenic eclogite is not governed by the metamorphic peak conditions, at least not in the PT range of 20–30 kbar and 600–900°C. This is in contrast to garnet from the same set of samples showing extremely low H_2O contents in quartz eclogite (most samples <2–50 ppm) and significantly higher values in coesite eclogite (50–150 ppm; e.g., Gose & Schmädicke, 2018). The latter finding agrees with the results of HP experiments showing that the uptake of H_2O in garnet is enhanced by pressure (Lu & Keppler, 1997). However, in the case of EG and FG eclogite, the grossular content and the co-stability of hydrous minerals in the PT peak assemblage have been demonstrated to be the main reasons for the contrasting H_2O contents in garnet (Gose & Schmädicke, 2018). For omphacite, such a relation is not observed. Regardless of

whether peak-metamorphic, late- and/or post-eclogitic hydrous minerals occur the H_2O content of omphacite is as high as in samples without such phases.

The present study provides new clues concerning the influence of the PT conditions on structural H_2O in natural omphacite, which is important information because experimental data in this context are sparse and restricted to end-member compositions and binary solid solutions. Experiments on pure jadeite indicate that, in contrast to garnet, H_2O incorporation decreases with pressure, from 450 ppm at 2 GPa to 100 ppm at 10 GPa (Bromiley & Keppler, 2004), but it remains uncertain if such a relation also applies to more complex compositions. The same study showed that a binary solid solution of jadeite–Ca-Eskola component is able to incorporate much more H_2O (780 ppm at 20 kbar) than pure jadeite (Bromiley & Keppler, 2004). Also, data from natural samples (i.e., Pohorje eclogite; Skogby et al., 2016) show a positive correlation between H_2O and the amount of Ca-Eskola component in omphacite. Bromiley and Keppler (2004) concluded that pyroxene composition is more important in the present context than P and T. Although the Ca-Eskola component can only play a minor role in our samples, our results agree with the suggestion that H_2O incorporation in pyroxene is strongly influenced by its composition. In the present case, H_2O in omphacite correlates positively with Ti, tetrahedral Al, and diopside component and negatively with jadeite content but not with P or T. Particularly, the varying Na and Ti contents in omphacite from Erzgebirge eclogite can be reconciled with variations of the bulk rock composition (Schmädicke, 1994; Schmädicke & Will, 2021).

The finding that the H_2O content of omphacite neither differs between quartz and coesite eclogite nor between quartz eclogite samples with different peak conditions (i.e., 20–22 kbar/650°C and 24–26 kbar/750°C) has far-reaching implications. (i) It suggests that all H_2O in omphacite was incorporated in the quartz stability field, most probably, during mineral growth due to the transition of HP garnet amphibolite to eclogite. The related metamorphic reactions involved dehydration of the large amounts of amphibole, providing for H_2O in excess to be taken up by the newly formed omphacite. In addition, the failure to take up more H_2O with increasing PT conditions implies (ii) that the measured concentrations may be equal to the H_2O storage capacity of the studied omphacite and (iii) that this capacity remains unchanged during further PT increase. This does not exclude that omphacite from other occurrences with slightly different composition, especially more Ca-Eskola component, may take up more water (see Section 6.2).

In contrast to omphacite, most H_2O in garnet was derived from the final breakdown of the last remaining calcic amphibole close to the coesite stability field (Gose & Schmädicke, 2018). This conclusion is based on the much higher H_2O content in garnet from coesite eclogite (up to 180 ppm) versus quartz eclogite (up to 50 ppm).

A simple estimation helps to evaluate how much of the water released by dehydration reactions during the amphibolite-eclogite transition and, later on, due to PT increase within the eclogite facies can be recycled into the mantle by the subduction of coesite eclogite (Table 5). Omphacite with an average H_2O content of 800 ppm and a modal amount of 60 vol.% hosts 480 ppm of the bulk rock H_2O—a quantity equivalent to that in ~2.5 vol.% calcic amphibole (and/or zoisite). The maximum H_2O content of omphacite in our study (1,100 ppm) translates to 660 ppm bulk rock water, corresponding to 3.3 vol.% amphibole (and/or zoisite). Adding the H_2O amount hosted by garnet (50 ppm), the bulk rock content of quartz eclogite is only slightly higher, that is, 500 ppm (average) and 680 ppm (maximum), respectively.

Coesite eclogite with up to 180 ppm H_2O in garnet (Gose & Schmädicke, 2018) contains somewhat more

TABLE 5 Estimation of the water content in quartz and coesite eclogite based on the data for omphacite (this study) and garnet (Gose & Schmädicke, 2018) and a modal composition of 60% omphacite and 40% garnet

		Quartz eclogite H_2O (ppm)	Coesite eclogite H_2O (ppm)
Garnet	max	50	180
In 40% garnet	max	20	70
Omphacite	avg	800	800
	max	1,100	1,100
In 60% omphacite	avg	480	480
	max	660	660
Eclogite	avg	500	550
	max	680	730

Abbreviations: avg, average; max, maximum.

H_2O (average: 550 ppm, maximum: 730 ppm; Table 5). The 50 ppm increase of bulk rock storage capacity, from quartz to coesite eclogite, is very small compared with the 1,000–2,000 ppm H_2O released by 2.5–5 vol.% of each amphibole and zoisite that dehydrated between 25 and 30 kbar (Gose & Schmädicke, 2018). These authors argued that, for kinetic reasons, garnet failed to take up water from zoisite breakdown, mainly because this reaction is discontinuous and, therefore, all water is released in a single step, favouring its escape from the reaction site and the system. Zoisite decomposition, however, led to a 10 mol.% increase in grossular content, enhancing the ability of garnet to take up H_2O from the subsequent, continuous breakdown of the last remaining calcic amphibole, which decomposed close to the quartz-coesite transition (Gose & Schmädicke, 2018). The amphibole amount accounting for the difference of garnet H_2O contents in quartz versus coesite eclogite is only ~0.2–0.3 vol.%.

In conclusion, the maximum total amount of H_2O stored in the NAMs of coesite eclogite (730 ppm) well agrees with the 600 ppm estimated for the relatively dry 'HIMU' mantle component formed from subducted oceanic crust (Dixon et al., 2002). The 730 ppm bulk rock water correspond to ~3.6 vol.% hydrous minerals, such as amphibole and zoisite (with ~2 wt% H_2O). This value is significantly lower compared with the 5–10 vol.% hydrous minerals observed in quartz eclogite, which dehydrated between 25 and 30 kbar, let alone of the estimated 20–50 vol.% hydrous minerals that decomposed during the amphibolite-eclogite transition. Thus, most water was released from the subducting mafic rocks and liberated to the mantle wedge. Despite this, coesite eclogite consisting only of NAMs was able to preserve an H_2O amount equivalent to that in 3.6 vol.% amphibole (or zoisite) and transport it to depths of >100 km during further subduction. Even if the H_2O storage capacity of omphacite declines at $P > 30$ kbar, the effect is expected to be counter-balanced by the ability of natural garnet to incorporate more H_2O with increasing pressure (Lu & Keppler, 1997).

ACKNOWLEDGEMENTS

We are indebted to Helene Brätz (Erlangen) for help with the ICP analyses and to Roland Stalder (Innsbruck) for fruitful discussion and for providing the analytical facilities for the IR measurements. Funding by Deutsche Forschungsgemeinschaft (grant Schm1039/9-3) is gratefully acknowledged. We also like to thank Bernardo Cesare for editorial handling and valuable suggestions and to Bogdana Radu and István Kovács for their constructive and helpful reviews.

ORCID

Esther Schmädicke https://orcid.org/0000-0002-0522-8210

REFERENCES

Bell, D. R., Ihinger, P. D., & Rossman, G. R. (1995). Quantitative analysis of trace OH in garnet and pyroxenes. *American Mineralogist*, 80, 465–474. https://doi.org/10.2138/am-1995-5-607

Bell, D. R., & Rossman, G. R. (1992a). Water in the Earth's mantle: The role of nominally anhydrous minerals. *Science*, 255, 1391–1397. https://doi.org/10.1126/science.255.5050.1391

Bell, D. R., & Rossman, G. R. (1992b). The distribution of hydroxyl in garnets from the subcontinental mantle of southern Africa. *Contributions to Mineralogy and Petrology*, 111, 161–178. https://doi.org/10.1007/BF00348949

Bromiley, G. D., & Keppler, H. (2004). An experimental investigation of hydroxyl solubility in jadeite and Na-rich clinopyroxenes. *Contributions to Mineralogy and Petrology*, 147, 189–200. https://doi.org/10.1007/s00410-003-0551-1

Danyushevski, L. V., Eggins, S. M., Falloon, T. J., & Christie, D. M. (2000). H_2O abundance in depleted to moderately enriched mid-ocean ridge magmas; part I: Incompatible behaviour, implications for mantle storage, and origin of regional variations. *Journal of Petrology*, 41, 1329–1364. https://doi.org/10.1093/petrology/41.8.1329

Dixon, J. E., Leist, L., Langmuir, C., & Schilling, J. G. (2002). Recycled dehydrated lithosphere observed in plume-influenced mid-ocean-ridge basalt. *Nature*, 420, 385–389. https://doi.org/10.1038/nature01215

Frost, D. J. (2006). The stability of hydrous mantle phases. In *Reviews in mineralogy and geochemistry: Vol. 62. Water in nominally anhydrous minerals* (pp. 243–271). Mineralogical Society of America.

Gebauer, D., & Grünenfelder, M. (1979). U-Pb zircon and Rb-Sr mineral dating of eclogites and their country rocks. Example: Münchberg Gneiss Massif, Northeast Bavaria. *Earth and Planetary Science Letters*, 42, 35–44. https://doi.org/10.1016/0012-821X(79)90188-2

Gose, J., & Schmädicke, E. (2018). Water Incorporation in Garnet: Coesite versus Quartz Eclogite from Erzgebirge and Fichtelgebirge. *Journal of Petrology*, 59, 207–232. https://doi.org/10.1093/petrology/egy022

Gose, J., & Schmädicke, E. (2021). Water in the supra-subduction-zone mantle of the Mariana-Izu-Bonin forearc: Constraints from peridotitic orthopyroxene. *Geochemistry, Geophysics, Geosystems*, 1–22. https://doi.org/10.1029/2020GC009586

Grant, K., Ingrin, J., Lorand, J. P., & Dumas, P. (2007). Water partitioning between mantle minerals from peridotite xenoliths. *Contributions to Mineralogy and Petrology*, 154, 15–34. https://doi.org/10.1007/s00410-006-0177-1

Grant, K., Kohn, S. C., & Brooker, R. A. (2006). Solubility and partitioning of water in synthetic forsterite and enstatite in the system $MgO\text{-}SiO_2\text{-}H_2O\pm Al_2O_3$. *Contributions to Mineralogy and Petrology*, 151, 651–664. https://doi.org/10.1007/s00410-006-0082-7

Green, D. H., Hibberson, W. O., Rosenthal, A., Kovács, I., Yaxley, G. M., Falloon, T. J., & Brink, F. (2014). Experimental study of the influence of water on melting and phase

assemblages in the upper mantle. *Journal of Petrology*, 55, 2067–2096. https://doi.org/10.1093/petrology/egu050

Hirschmann, M. M., Aubaud, C., & Withers, A. C. (2005). Storage capacity of H_2O in nominally anhydrous minerals in the upper mantle. *Earth and Planetary Science Letters*, 236, 167–181. https://doi.org/10.1016/j.epsl.2005.04.022

Huang, J.-X., Li, P., Griffin, W. K., Xia, Q.-K., Gréau, Y., Pearson, N. J., & O'Reilly, S. Y. (2014). Water contents of Roberts Victor xenolithic eclogites: Primary and metasomatic controls. *Contributions to Mineralogy and Petrology*, 168, 1092. https://doi.org/10.1007/s00410-014-1092-5

Kang, P., Lamb, W. M., & Drury, M. (2017). Using mineral equilibria to estimate H_2O activities in peridotites from the Western Gneiss Region of Norway. *American Mineralogist*, 102, 1021–1036. https://doi.org/10.2138/am-2017-5915

Katayama, I., & Nakashima, S. (2003). Hydroxyl in clinopyroxene from the deep subducted crust: Evidence for H_2O transport into the mantle. *American Mineralogist*, 68, 229–234. https://doi.org/10.2138/am-2003-0126

Katayama, I., Nakashima, S., & Yurimoto, H. (2006). Water content in natural eclogite and implication for water transport into the deep upper mantle. *Lithos*, 86, 245–259. https://doi.org/10.1016/j.lithos.2005.06.006

Klemd, R., & Schmädicke, E. (1994). High-pressure metamorphism in the Münchberg Gneiss Complex and the Erzgebirge Crystalline Complex: The roles of fluid and reaction kinetics. *Geochemistry - Chemie der Erde*, 54, 241–261.

Koch-Müller, M., Abs-Wurmbach, I., Rhede, D., Kahlenberg, V., & Matsyuk, S. (2007). Dehydration experiments on natural omphacites: Qualitative and quantitative characterization by various spectroscopic methods. *Physics and Chemistry of Minerals*, 34, 663–678. https://doi.org/10.1007/s00269-007-0181-7

Koch-Müller, M., Matsyuk, S. S., & Wirth, R. (2004). Hydroxyl in omphacites and omphacitic clinopyroxenes of upper mantle to lower crustal origin beneath the Siberian platform. *American Mineralogist*, 89, 921–931. https://doi.org/10.2138/am-2004-0701

Kohlstedt, D. L., Keppler, H., & Rubie, D. C. (1996). Solubility of water in the α, β and γ phase of $(Mg,Fe)_2SiO_4$. *Contributions to Mineralogy and Petrology*, 123, 345–357. https://doi.org/10.1007/s004100050161

Konzett, J., Libowitzky, E., Hejny, C., Miller, C., & Zanetti, A. (2008). Oriented quartz+calcic amphibole inclusions in omphacite from the Saualpe and Pohorje Mountain eclogites, Eastern Alps—An assessment of possible formation mechanisms based on IR- and mineral chemical data and water storage in Eastern Alpine eclogites. *Lithos*, 106, 335–350. https://doi.org/10.1016/j.lithos.2008.09.002

Kovács, I., Hermann, J., O'Neill, H. S. C., Gerald, J. F., Sambridge, M., & Horváth, G. (2008). Quantitative absorbance spectroscopy with unpolarized light: Part II. Experimental evaluation and development of a protocol for quantitative analysis of mineral IR spectra. *American Mineralogist*, 93, 765–778. https://doi.org/10.2138/am.2008.2656

Libowitzky, E., & Beran, A. (2006). The structure of hydrous species in nominally anhydrous minerals: Information from polarized IR spectroscopy. In H. Keppler & H. R. Smyth (Eds.), *Water in nominally anhydrous minerals* (Vol. 62) (pp. 29–52). Mineralogical Society of America.

Libowitzky, E., & Rossman, G. R. (1997). An IR absorption calibration for water in minerals. *American Mineralogist*, 82, 1111–1115. https://doi.org/10.2138/am-1997-11-1208

Lu, R., & Keppler, H. (1997). Water solubility in pyrope to 100 kbar. *Contributions to Mineralogy and Petrology*, 129, 35–42. https://doi.org/10.1007/s004100050321

Massonne, H.-J. (2001). First find of coesite in the ultrahigh-pressure metamorphic region of the Central Erzgebirge, Germany. *European Journal of Mineralogy*, 13, 565–570. https://doi.org/10.1127/0935-1221/2001/0013-0565

McDonough, W. F., & Sun, S. S. (1995). The composition of the Earth. *Chemical Geology*, 120, 223–253. https://doi.org/10.1016/0009-2541(94)00140-4

Miller, G. H., Rossman, G. R., & Harlow, G. E. (1987). The natural occurrence of hydroxide in olivine. *Physics and Chemistry of Minerals*, 14, 461–472. https://doi.org/10.1007/BF00628824

Nasdala, L., & Massonne, H.-J. (2000). Microdiamonds from the Saxonian Erzgebirge, Germany: In situ micro-Raman characterization. *European Journal of Mineralogy*, 12, 495–498. https://doi.org/10.1127/0935-1221/2000/0012-0495

Niida, K., & Green, D. H. (1999). Stability and chemical composition of pargasitic amphibole in MORB pyrolite under upper mantle conditions. *Contributions to Mineralogy and Petrology*, 135, 18–40. https://doi.org/10.1007/s004100050495

O'Brien, P. J. (1993). Partially retrograded eclogites from the Münchberg Massif Germany: Records of a multistage Variscan uplift history in the Bohemian Massif. *Journal of Metamorphic Geology*, 11, 241–260. https://doi.org/10.1111/j.1525-1314.1993.tb00145.x

Patkó, L., Liptai, N., Kovács, I. J., Aradi, L. I., Xia, Q.-K., Ingrin, J., Mihály, J., O'Reilly, S. Y., Griffin, W. L., Wesztergom, V., & Szabó, C. (2019). Extremely low structural hydroxyl contents in upper mantle xenoliths from the Nógrád-Gömör volcanic field (northern Pannonian Basin): Geodynamic implications and the role of post-eruptive re-equilibration. *Chemical Geology*, 507, 23–41. https://doi.org/10.1016/j.chemgeo.2018.12.017

Pawley, A. R., & Holloway, J. R. (1993). Water sources in subduction zone volcanism: New experimental constraints. *Science*, 260, 664–667. https://doi.org/10.1126/science.260.5108.664

Purwin, H., Stalder, R., & Skogby, H. (2009). Hydrogen incorporation in Fe- and Na-doped diopsides. *European Journal of Mineralogy*, 21, 691–704. https://doi.org/10.1127/0935-1221/2009/0021-1938

Rauch, M., & Keppler, H. (2002). Water solubility in orthopyroxene. *Contributions to Mineralogy and Petrology*, 143, 525–536. https://doi.org/10.1007/s00410-002-0365-6

Sambridge, M., Gerald, J. F., Kovács, I., O'Neill, H. S. C., & Hermann, J. (2008). Quantitative absorbance spectroscopy with unpolarized light: Part I. Physical and mathematical development. *American Mineralogist*, 93, 751–764. https://doi.org/10.2138/am.2008.2657

Schmädicke, E. (1991). Quartz pseudomorphs after coesite in eclogites from the Saxonian Erzgebirge. *European Journal of Mineralogy*, 3, 231–238. https://doi.org/10.1127/ejm/3/2/0231

Schmädicke, E. (1994). Die Eklogite des Erzgebirges. In *Vol. C 456. Freiberger Forschungsheft* (p. 338). Deutscher Verlag für Grundstoffindustrie.

Schmädicke, E., & Evans, B. W. (1997). Garnet-bearing ultramafic rocks from the Erzgebirge, and their relation to other settings

in the Bohemian Massif. *Contributions to Mineralogy and Petrology*, 127, 57–74. https://doi.org/10.1007/s004100050265

Schmädicke, E., & Gose, J. (2017). Water transport by subduction: Clues from garnet of Erzgebirge UHP eclogite. *American Mineralogist*, 102, 975–986. https://doi.org/10.2138/am-2017-5920

Schmädicke, E., & Gose, J. (2020). Water in garnet of garnetite (metarodingite) and eclogite from the Erzgebirge and the Lepontine Alps. *Journal of Metamorphic Geology*, 38, 905–933. https://doi.org/10.1111/jmg.12554

Schmädicke, E., Gose, J., Reinhardt, J., Will, T. M., & Stalder, R. (2015). Garnet in cratonic and non-cratonic mantle and lower crustal xenoliths from southern Africa: Composition, water incorporation and geodynamic constraints. *Precambrian Research*, 270, 285–299. https://doi.org/10.1016/j.precamres.2015.09.019

Schmädicke, E., Mezger, K., Cosca, M. A., & Okrusch, M. (1995). Variscan Sm-Nd and Ar-Ar ages of eclogite-facies rocks from the Erzgebirge, Bohemian Massif. *Journal of Metamorphic Geology*, 13, 537–552. https://doi.org/10.1111/j.1525-1314.1995.tb00241.x

Schmädicke, E., & Müller, W. F. (2000). Unusual exsolution phenomena in omphacite and partial replacement of phengite by phlogopite + kyanite in an eclogite from the Erzgebirge. *Contributions to Mineralogy and Petrology*, 139, 629–642. https://doi.org/10.1007/s004100000161

Schmädicke, E., Okrusch, M., & Schmidt, W. (1992). Eclogite-facies rocks in the Saxonian Erzgebirge, Germany: High pressure metamorphism under contrasting P-T conditions. *Contributions to Mineralogy and Petrology*, 110, 226–241. https://doi.org/10.1007/BF00310740

Schmädicke, E., & Will, T. (2021). No chemical change during high-T dehydration and re-hydration reactions: Constraints from Erzgebirge HP and UHP eclogite. *Lithos*, 386-387, 105995. https://doi.org/10.1016/j.lithos.2021.105995

Schmädicke, E., Will, T. M., Ling, X., Li, X.-H., & Li, Q.-L. (2018). Rare peak and ubiquitous post-peak zircon in eclogite: Constraints for the timing of UHP and HP metamorphism in Erzgebirge, Germany. *Lithos*, 322, 250–267. https://doi.org/10.1016/j.lithos.2018.10.017

Skogby, H. (2006). Water in natural mantle minerals I: Pyroxenes. In *Reviews in mineralogy and geochemistry: Vol. 62. Water in nominally anhydrous minerals* (pp. 155–167). Mineralogical Society of America.

Skogby, H., Bell, D. R., & Rossman, G. R. (1990). Hydroxide in pyroxene: Variations in the natural environment. *American Mineralogist*, 75, 764–774.

Skogby, H., Janák, M., & Broska, I. (2016). Water incorporation in omphacite: Concentrations and compositional relations in ultrahigh-pressure eclogites from Pohorje, Eastern Alps. *European Journal of Mineralogy*, 28, 631–639. https://doi.org/10.1127/ejm/2016/0028-2533

Smyth, J. R., Bell, D. R., & Rossman, G. R. (1991). Incorporation of hydroxyl in upper-mantle clinopyroxene. *Nature*, 351, 732–735. https://doi.org/10.1038/351732a0

Stalder, R. (2021). OH point defects in quartz—A review. *European Journal of Mineralogy*, 33, 145–163. https://doi.org/10.5194/ejm-33-145-2021

Stalder, R., Karimova, A., & Konzett, J. (2015). OH-defects in multiple-doped orthoenstatite at 4-8 GPa: the gap between pure and natural systems. *Contributions to Mineralogy and Petrology*, 169, 38. https://doi.org/10.1007/s00410-015-1133-8

Stalder, R., & Ludwig, T. (2007). OH incorporation in synthetic diopside. *European Journal of Mineralogy*, 19, 373–380. https://doi.org/10.1127/0935-1221/2007/0019-1721

Stöckhert, B., Duyster, J., Trepmann, C., & Massonne, H. J. (2001). Microdiamond daughter crystals precipitated from supercritical COH silicate fluids included in garnet, Erzgebirge, Germany. *Geology*, 29, 391–394. https://doi.org/10.1130/0091-7613(2001)029%3C0391:MDCPFS%3E2.0.CO;2

Stosch, H. G., & Lugmair, G. W. (1990). Geochemistry and evolution of MORB-type eclogites from the Münchberg Massif, southern Germany. *Earth and Planetary Science Letters*, 99, 230–249. https://doi.org/10.1016/0012-821X(90)90113-C

van Achterbergh, E., Ryan, C. G., & Griffin, W. L. (2000). *GLITTER: On-line interactive data reduction for the Laser Ablation ICPMS microprobe*. Macquarie University.

Withers, A. C., & Hirschmann, M. M. (2007). H_2O storage capacity of $MgSiO_3$ clinoenstatite at 8–13 GPa, 1,100–1,400 °C. *Contributions to Mineralogy and Petrology*, 154, 663–664. https://doi.org/10.1007/s00410-007-0215-7

Withers, A. C., Wood, B. J., & Carroll, M. R. (1998). The OH content of pyrope at high pressure. *Chemical Geology*, 147, 161–171. https://doi.org/10.1016/S0009-2541(97)00179-4

SUPPORTING INFORMATION

Additional supporting information may be found in the online version of the article at the publisher's website.

Figure S1 IR absorption spectrum of phengite from Erzgebirge eclogite normalized to 1 cm sample thickness.
Table S1 Standard deviations of microprobe analyses.
Table S2 Standard deviations of ICP-MS analyses.

How to cite this article: Gose, J. & Schmädicke, E. (2022) H_2O in omphacite of quartz and coesite eclogite from Erzgebirge and Fichtelgebirge, Germany. *Journal of Metamorphic Geology*, 40(4), 665–686. Available from: https://doi.org/10.1111/jmg.12642